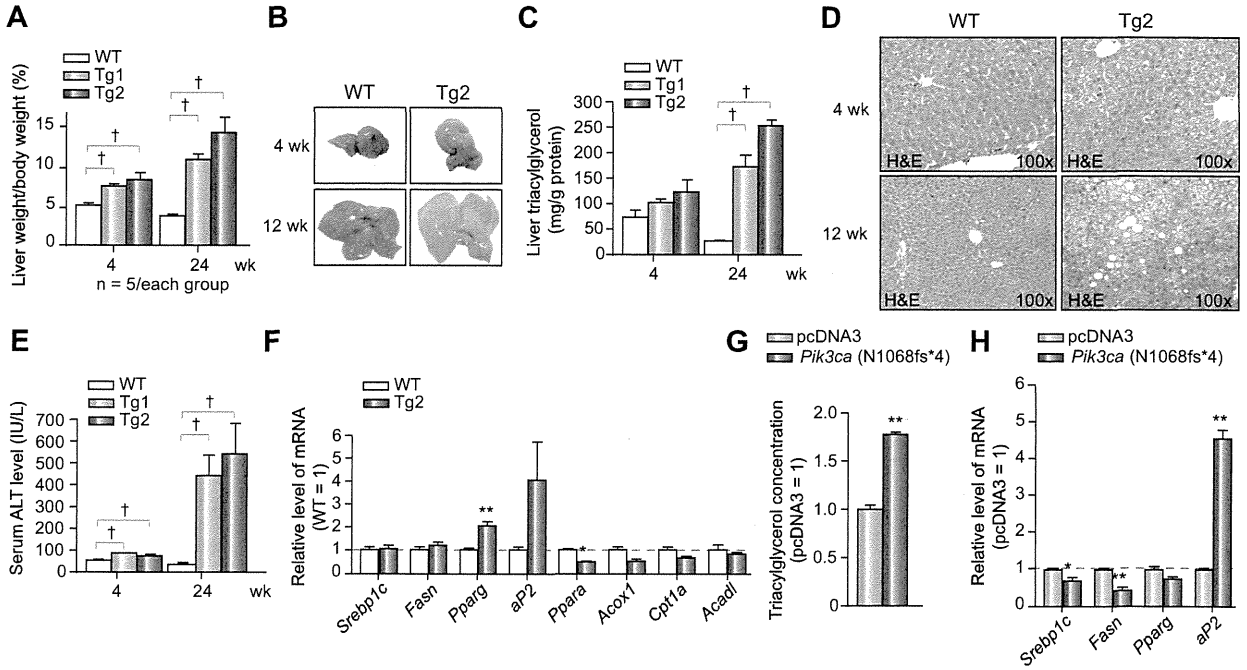

Fig. 2. Steatosis in the *Pik3ca* Tg liver. (A) Increased liver weight in *Pik3ca* Tg mice. (N = 5/group; †p <0.05, ANOVA; post hoc test with WT). (B) Representative liver images of WT and *Pik3ca* Tg mice. (C) High concentrations of intrahepatic triacylglycerol in the Tg mice (N >5/group; †p <0.05, ANOVA; post hoc test with WT). (D) H&E staining of livers from WT and *Pik3ca* Tg mice at 4 weeks (top) and 24 weeks (bottom) of age. (E) Higher serum ALT levels in the Tg mice (N = 5/group; †p <0.05, ANOVA; post hoc test with WT). (F) The expression of fat metabolism genes in the 4-week-old liver (N = 3–4/group; *p <0.05, **p <0.01, Student's t-test). (G) Cellular triacylglycerol levels and (H) the expression of lipogenesis-related genes in BNL-CL2 cells stably expressing *Pik3ca* (N1068fs*4) (N = 3/group; *p <0.05, **p <0.01, Student's t-test).

oncogenic activity in itself [13] and that there might be unknown factors promoting *in vivo* tumorigenesis in the *Pik3ca* Tg liver.

Downregulation of tumor suppressor genes in tumors derived from Pik3ca Tg livers

To further assess the related cellular signaling for tumorigenesis in the *Pik3ca* liver, we evaluated the activation of Akt, S6K, and Erk among the WT liver, non-tumor Tg liver, and tumor tissues from 52-week-old mice (Fig. 4A). Tumor tissues exhibited significantly enhanced activation of Akt compared to the Akt activation in non-tumor background or WT livers. We observed stronger phosphorylation of Akt in the non-tumor Tg liver than in WT livers, but the difference was not statistically significant as determined by ANOVA. Furthermore, the immunohistochemistry for phospho-Akt did not demonstrate clear differences between non-tumor livers and WT tissues. In contrast, the expression of *Myc-Pik3ca* was sustained in the non-tumor liver at 52 weeks (Supplementary Fig. 7). Those findings suggest the possibility that continuous activation of Akt induced by overexpressed *Pik3ca* is important for tumor formation in the Tg livers [31], whereas it remains unknown why Akt phosphorylation was attenuated in the non-tumor liver at 52 weeks despite the sustained expression of *Pik3ca* (Fig. 4A and Supplementary Fig. 7). In addition, the phosphorylation of S6K and Erk tended to be higher in Tg livers than in WT livers (Fig. 4A), but the difference became attenuated at 52 weeks compared to that at 4 weeks (Figs. 1B and 4A and Supplementary Fig. 8). These data do not exclude the possible role of these molecules in tumorigenesis in Tg livers but at least may emphasize the importance of Akt activation. Next, we examined the expression levels of genes involved in murine hepatotumorigenesis [32–34]. We observed decreased expression of four tumor suppressor genes, *Pten*, AT-rich interactive domain 5B (*Arid5b*), exportin 4 (*Xpo4*), and deleted in liver cancer 1 (*Dlc1*), in the tumor compared to the non-tumor background of *Pik3ca* Tg livers (Fig. 4B and Supplementary Fig. 9). PTEN protein levels were downregulated (Fig. 4C). To address whether the downregulation of *Pten* contributes to the tumorigenic activity in liver cells, we established *Pten*-depleted BNL-CL2 cells (Fig. 4D). *Pten*-depleted BNL-CL2 cells generated significantly more colonies in soft agar (Fig. 4E), indicative of enhanced tumorigenicity. These findings emphasize the possibility that the decreased expression of tumor suppressor genes has a certain role in tumorigenesis in the *Pik3ca* Tg liver. Importantly, the *in vitro* overexpression of mutant *Pik3ca* (N1068fs*4) only suppressed *Arid5b* expression but did not decrease the expression of *Pten*, *Xpo4*, or *Dlc1* in BNL-CL2 cells, indicating that certain additional mechanisms repressed their expression (Supplementary Fig. 10). Although several reports suggested a relationship between oxidative stress and hepatocarcinogenesis [35], the levels of hydrogen peroxide and lipid peroxidation were comparable between Tg and WT livers (Supplementary Fig. 11).

Tumors contain higher concentrations of OAs and palmitic acids (PAs) compared to the background tissues in the Pik3ca Tg liver

Recent intensive research has shed light into the significance of fatty acid (FA) as a potent biological stimulator of intracellular

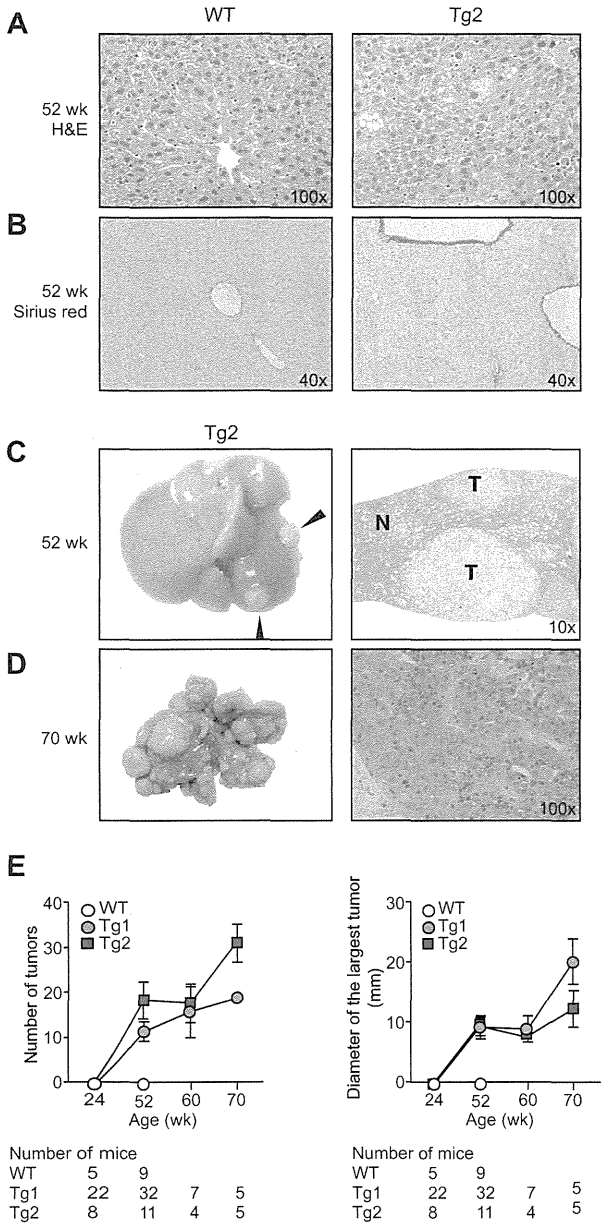

Fig. 3. Liver tumors in the *Pik3ca* Tg mice. (A) H&E and (B) Sirius red staining of livers at 52 weeks. (C) Macroscopic view (left) of the representative liver adenomas (arrowheads) at 52 weeks of age. H&E staining of an adenoma (T) and adjacent parenchyma (N) (right). (D) Tumors in *Pik3ca* Tg mice at 70 weeks (left). H&E staining of HCC (right). (E) The number (left) and size (right) of hepatic tumors. The number of mice examined is shown below the graphs.

signaling [36]. Interestingly, unsaturated FAs inhibit *Pten* expression via microRNA-21 in hepatoma [7,37,38], and the overexpression of a FA receptor (FFAR2) transformed the 3T3 fibroblasts [39], suggesting the possible relationship between FA and tumorigenesis. In the *Pik3ca* Tg liver, the tumor tissues contained higher concentrations of FAs than the non-tumor background tissues (Fig. 5A). The difference in total FA levels was largely due to the increase in levels of OA (C18:1n9) and PA (C16:0) in the tumors (Fig. 5B and C, Supplementary Fig. 12 and Table 2).

OA has the potential to repress the expression of tumor suppressors and enhance colony formation in vitro

To examine the possibility that either OA or PA downregulates the expression of tumor suppressors including *Pten*, we treated BNL-CL2 cells with OA or PA. OA, but not PA, repressed the expression of *Pten*, *Arid5b*, *Xpo4*, and *Dlc1* (Fig. 6A). Moreover, BNL-CL2 cells exposed to OA formed significantly more colonies in soft agar (Fig. 6B). These findings indicate that OA potentially enhances the in *vivo* tumorigenesis in the *Pik3ca* Tg liver. As an example, it is likely that decreased PTEN expression could enhance the Akt activation by the *Pik3ca* transgene in Tg-derived tumors (Fig. 1B).

Discussion

Hepatocyte-specific overexpression of *Pik3ca* (N1068fs*4) leads to steatosis and hepatic tumor formation. This mutation was originally isolated in human HCC and gastric cancers [12], but its functional analysis has never been reported. The *in vitro* overexpression of this mutant clearly induced Akt activation, but the level of activation was comparable with that of *Pik3ca* wild type and lower than that of the oncogenic H1047R mutant, suggesting that the *Pik3ca* Tg mice provide a model for studying effects of PIK3CA overexpression rather than a gain-of-function of PIK3CA. Furthermore, the N1068fs*4 mutation was not sufficient for cellular transformation *in vitro*, different from *Pik3ca* H1047R [40]. Considering results from a previous report suggesting the pivotal role of Akt activation in cell transformation by *PIK3CA* mutation [13], the activation level of Akt induced by *Pik3ca* (N1068fs*4) expression should not be sufficient for the cell-transforming process. These data indicated that the development of hepatic tumors in Tg mice might not be always a direct effect of *Pik3ca* (N1068fs*4) but instead promoted by other *in vivo* protumorigenic factors.

We focused on FA as an additional protumorigenic factor contributing to *in vivo* hepato-tumorigenesis in Tg mice, based on recent research on their oncogenic capacity [39]. Previous studies reported that OA inhibits *PTEN* expression via the upregulation of microRNA-21 through an mTOR/NF-κB-dependent mechanism [37,38] and also that exposure to OA increases tumor growth in xenografts [7]. Here, we demonstrated the correlation between OA accumulation and downregulation of other tumor suppressors, whereas the entire molecular mechanism remains to be elucidated. At least, there is a possibility that, in the Tg-derived tumors, OA accumulation enhanced the Akt activation by the *Pik3ca* transgene, which phosphorylates Akt less strongly than other oncogenic mutants *in vitro* (Fig. 1B, Supplementary Figs. 6 and 13).

Lipogenesis is mainly mediated by two major transcription factors, PPARγ and SREBP1C [24,25]. Hepatocyte-specific *Pten* KO mice exhibited increased expression of both PPARγ and SREBP1c in the liver, whereas only PPARγ was highly expressed in the *Pik3ca* Tg liver [16]. Our *in vitro* data suggested that the PI3K signaling is upstream of the activation of PPARγ in hepatocytes. A recent study shows that levels of *PPARγ* as well as *SREBP1c* mRNA are higher in the livers of patients with steatosis

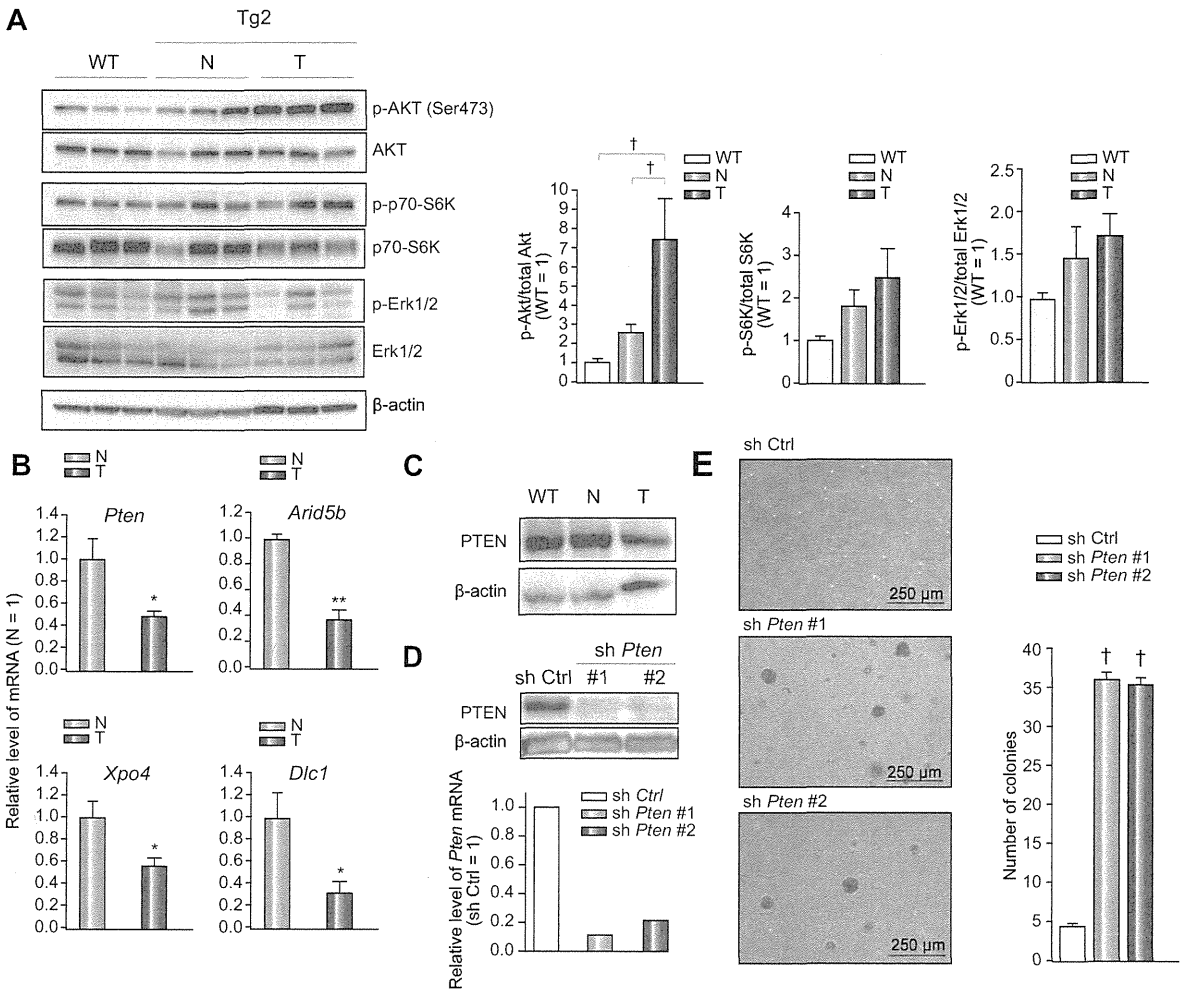

Fig. 4. *Pten* downregulation in the *Pik3ca* Tg liver. (A) Immunoblots and quantification of liver homogenates at 52 weeks (†p <0.05, ANOVA; post hoc test with WT). (B) The decreased expression of *Pten*, *Arid5b*, *Xpo4*, and *Dlc1* mRNA in the *Pik3ca* Tg liver tumors (T) relative to their expression in background liver tissues (N) (N = 5/group; *p <0.05, **p <0.01, Student's t-test). (C) Representative images of immunoblots of liver tissues from the littermates at 52 weeks. (D) Knockdown of *Pten* in BNL-CL2 cells confirmed at the protein (top) and mRNA (bottom) levels. (E) Both lines of *Pten*-depleted BNL-CL2 cells (sh*Pten* #1 and #2) formed more colonies in soft agar (N = 3/group; †p <0.05, ANOVA; post hoc test with control cells (shCtrl)).

or steatohepatitis, suggesting that the activity of PPARγ is implicated in the abnormal lipid accumulation in human livers [41] (Supplementary Fig. 13).

Unlike the hepatocyte-specific *Pten* KO mice [16], cellular infiltration and fibrosis were not observed in the *Pik3ca* Tg liver. One explanation is the possibility that *Pten* deficiency induces certain pathological mechanisms independently of PI3K-Akt activation, as previously reported for mammary tumorigenesis [18–20,42–45]. Indeed, although genetic changes in PTEN result in potent Akt phosphorylation, *in vivo* studies have suggested that they show distinct phenotypes [42]. The conditional knockout of PTEN enhanced tumorigenesis in the mammary gland [43]; however, transgenic mice expressing constitutively active Akt in the mammary gland did not show tumor formation [44]. PTEN directly associates with p53, thereby increasing its stability, protein level, and transcriptional activity [18,19]. PTEN induces apoptosis and cell cycle arrest through PI3K/Akt-independent pathways [20]. PTEN also has important roles in integrin signaling and has the ability to dephosphorylate focal adhesion kinase, reducing cell adhesion and enhancing migration [46]. These findings support an alternative mechanism of PTEN-mediated tumorigenesis independent on PI3K/Akt pathway. As a second reason for the difference from *Pten* KO mice, it is possible that PI3K catalytic beta has a distinct role with PIK3CA in the phenotype of *Pten* deficiency [47].

The discrepancy between the scarce inflammatory levels in the *Pik3ca* Tg liver and the strong increase in serum ALT levels indicative of severe liver injury is to be solved in the near future. We found that inflammatory cytokine IL-1α and Fas ligand were more highly expressed in the *Pik3ca* Tg liver than in the WT liver (Supplementary Fig. 4). Taking into account reports demonstrating that these factors can lead to liver damage [28,29], it can be suggested that their abnormal upregulation in Tg livers is in part responsible for liver damage, whereas the entire molecular process inducing them remains unknown (Supplementary Fig. 13).

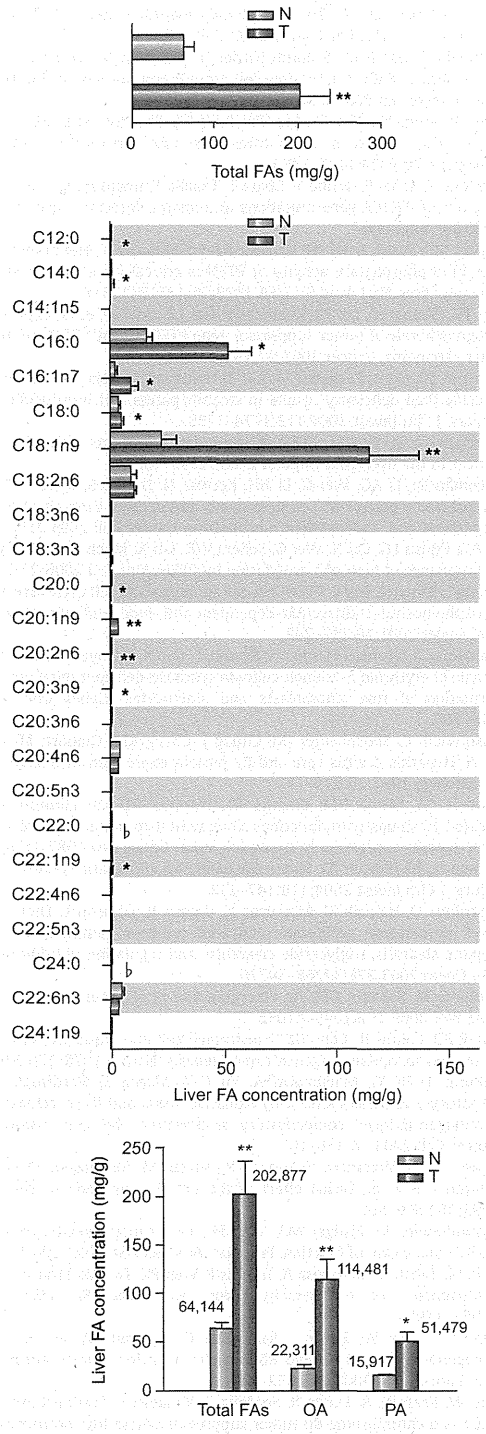

Fig. 5. The total FA composition in the *Pik3ca* Tg liver tissues and tumors. (A) The levels of FAs in the tumor (T) and non-tumor background tissue (N) in *Pik3ca* Tg mice at 52 weeks (N = 4/group; $^{**}p$ <0.01, Student's *t*-test). (B) FA composition in background (N) and tumor tissues (T) (N = 4/group; statistically increased FA levels in the tumors are shown with asterisks ($^{*}p$ <0.05, $^{**}p$ <0.01) and significantly decreased levels are shown with flat (μ, p <0.05), Student's *t*-test). (C) The concentration of total FAs, OA, and PA in background (N) and tumor tissues (T) (N = 4/group; $^{*}p$ <0.05, $^{**}p$ <0.01, Student's *t*-test).

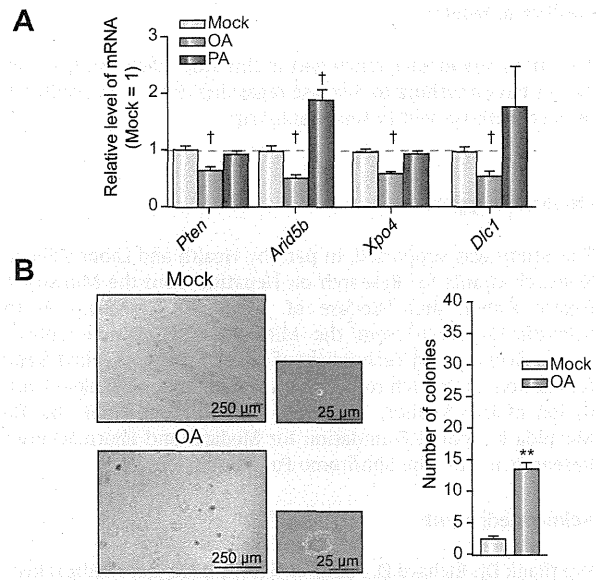

Fig. 6. OA enhances the colony-forming activity of immortalized hepatocytes. (A) OA but not PA decreased *Pten*, *Arid5b*, *Xpo4*, and *Dlc1* mRNA *in vitro* (N = 3/group; $^{\dagger}p$ <0.05, ANOVA; post hoc test with Mock group). (B) Colony formation assay of BNL-CL2 cells with or without 50 μmol/L OA in 10% or 0.5% FBS media (N = 3/group; $^{**}p$ <0.01, Student's *t*-test).

Mechanisms involved in the pathogenesis of non-alcoholic steatohepatitis (NASH) remain unclear, but the "two-hit theory" is widely accepted [48]. That is, in the first hit, insulin-resistance is followed by lipid accumulation in the liver, and the second hit, possibly involving inflammatory cytokines or oxidative stress, results in hepatic injury and fibrosis. It has been reported that ROS has certain roles in *in vivo* carcinogenesis [35], and the concentration of ROS is upregulated in the liver suffering NASH or NASH-derived HCC [49]. Regardless of the obvious fatty liver, our model mice have not shown impaired glucose tolerance. The concentration of ROS in the *Pik3ca* Tg mice was comparable with that of WT mice (Supplementary Fig. 11), which can be partly explained by the lower expression of fat-oxidative genes (Fig. 2F) and lack of inflammatory cell infiltration. These findings indicate that *Pik3ca* Tg mice do not always mimic the entire pathological mechanisms causing NASH, while they might be useful as a prototype to determine which pathological processes are required for the progression from the fatty liver to NASH. In addition, given the low rate of HCC development in these mice, they can be potentially useful for discovering tumor-promoting factors in hepatic steatosis. For example, although it was unlikely that ROS is involved in the initiation of hepatic tmor in the *Pik3ca* Tg liver, we can examine the pathological significance of ROS in tumor progression as well as hepatitis induction by applying the *Pik3ca* Tg liver to the condition producing high levels of ROS.

Recent clinical findings have advocated the relationship between volume of visceral fat and tumor progression [1–4]. While there is no direct molecular evidence to address the notion that abnormal body fat accumulation accelerates tumor growth, our data might provide new insights into the mechanisms of the "lipotoxicity-related" tumorigenesis. Future researches are needed to unravel how OA affects gene expression.

Conflict of interest

The authors who have taken part in this study declared that they do not have anything to disclose regarding funding or conflict of interest with respect to this manuscript.

Financial support

This study was supported, in part, by Health and Labor Sciences Research Grants for Research on Hepatitis from the Ministry of Health, Labor, and Welfare of Japan, by Grants-in-Aid for Scientific Research from the Ministry of Education, Culture, Sports, Science, and Technology of Japan, by The Mishima-Kaiun foundation, by the Ichiro Kanehara Foundation, by Sankyo Foundation of Life Science, by Takeda Science Foundation, by The Mochida Memorial Foundation for Medical and Pharmaceutical Research and by The Sumitomo Foundation.

Acknowledgments

We thank Dr. Richard D. Palmiter (Howard Hughes Medical Institute and Department of Biochemistry, University of Washington, Seattle, USA) and Francis V. Chisari (Department of Molecular and Experimental Medicine, Scripps Research Institute, La Jolla, USA) for providing the plasmid. We also thank Dr. Junji Shibahara (Department of Pathology, Graduate School of Medicine, The University of Tokyo) and Kojiro Ueki (Department of Metabolic Diseases, Graduate School of Medicine, The University of Tokyo) for helpful discussions, and Mitsuko Tsubouchi for technical assistance.

Supplementary data

Supplementary data associated with this article can be found, in the online version, at doi:10.1016/j.jhep.2011.03.025.

References

[1] Garfinkel L. Overweight and cancer. Ann Intern Med 1985;103:1034–1036.
[2] Deslypere JP. Obesity and cancer. Metabolism 1995;44:24–27.
[3] Schapira DV, Clark RA, Wolff PA, Jarrett AR, Kumar NB, Aziz NM. Visceral obesity and breast cancer risk. Cancer 1994;74:632–639.
[4] Yamaji Y, Okamoto M, Yoshida H, Kawabe T, Wada R, Mitsushima T, et al. The effect of body weight reduction on the incidence of colorectal adenoma. Am J Gastroenterol 2008;103:2061–2067.
[5] Hill-Baskin AE, Markiewski MM, Buchner DA, Shao H, DeSantis D, Hsiao G, et al. Diet-induced hepatocellular carcinoma in genetically predisposed mice. Hum Mol Genet 2009;18:2975–2988.
[6] Park EJ, Lee JH, Yu GY, He G, Ali SR, Holzer RG, et al. Dietary and genetic obesity promote liver inflammation and tumorigenesis by enhancing IL-6 and TNF expression. Cell 2010;140:197–208.
[7] Vinciguerra M, Carrozzino F, Peyrou M, Carlone S, Montesano R, Benelli R, et al. Unsaturated fatty acids promote hepatoma proliferation and progression through downregulation of the tumor suppressor PTEN. J Hepatol 2009;50:1132–1141.
[8] Engelman JA, Luo J, Cantley LC. The evolution of phosphatidylinositol 3-kinases as regulators of growth and metabolism. Nat Rev Genet 2006;7:606–619.
[9] Bader AG, Kang S, Zhao L, Vogt PK. Oncogenic PI3K deregulates transcription and translation. Nat Rev Cancer 2005;5:921–929.
[10] Vivanco I, Sawyers CL. The phosphatidylinositol 3-kinase AKT pathway in human cancer. Nat Rev Cancer 2002;2:489–501.
[11] Samuels Y, Diaz Jr LA, Schmidt-Kittler O, Cummins JM, Delong L, Cheong I, et al. Mutant PIK3CA promotes cell growth and invasion of human cancer cells. Cancer cell 2005;7:561–573.
[12] Lee JW, Soung YH, Kim SY, Lee HW, Park WS, Nam SW, et al. PIK3CA gene is frequently mutated in breast carcinomas and hepatocellular carcinomas. Oncogene 2005;24:1477–1480.
[13] Ikenoue T, Kanai F, Hikiba Y, Obata T, Tanaka Y, Imamura J, et al. Functional analysis of PIK3CA gene mutations in human colorectal cancer. Cancer Res 2005;65:4562–4567.
[14] Myers MP, Pass I, Batty IH, Van der Kaay J, Stolarov JP, Hemmings BA, et al. The lipid phosphatase activity of PTEN is critical for its tumor suppressor function. Proc Natl Acad Sci USA 1998;95:13513–13518.
[15] Hu TH, Huang CC, Lin PR, Chang HW, Ger LP, Lin YW, et al. Expression and prognostic role of tumor suppressor gene PTEN/MMAC1/TEP1 in hepatocellular carcinoma. Cancer 2003;97:1929–1940.
[16] Horie Y, Suzuki A, Kataoka E, Sasaki T, Hamada K, Sasaki J, et al. Hepatocyte-specific Pten deficiency results in steatohepatitis and hepatocellular carcinomas. J Clin Invest 2004;113:1774–1783.
[17] Vinciguerra M, Foti M. PTEN at the crossroad of metabolic diseases and cancer in the liver. Ann Hepatol 2008;7:192–199.
[18] Freeman DJ, Li AG, Wei G, Li HH, Kertesz N, Lesche R, et al. PTEN tumor suppressor regulates p53 protein levels and activity through phosphatase-dependent and -independent mechanisms. Cancer Cell 2003;3:117–130.
[19] Li AG, Piluso LG, Cai X, Wei G, Sellers WR, Liu X. Mechanistic insights into maintenance of high p53 acetylation by PTEN. Mol Cell 2006;23:575–587.
[20] Weng L, Brown J, Eng C. PTEN induces apoptosis and cell cycle arrest through phosphoinositol-3-kinase/Akt-dependent and -independent pathways. Hum Mol Genet 2001;10:237–242.
[21] Nakajima O, Okano S, Harada H, Kusaka T, Gao X, Hosoya T, et al. Transgenic rescue of erythroid 5-aminolevulinate synthase-deficient mice results in the formation of ring sideroblasts and siderocytes. Genes Cells 2006;11:685–700.
[22] Pasquinelli C, Shoenberger JM, Chung J, Chang KM, Guidotti LG, Selby M, et al. Hepatitis C virus core and E2 protein expression in transgenic mice. Hepatology 1997;25:719–727.
[23] Pinkert CA, Ornitz DM, Brinster RL, Palmiter RD. An albumin enhancer located 10 kb upstream functions along with its promoter to direct efficient, liver-specific expression in transgenic mice. Genes Dev 1987;1:268–276.
[24] Browning JD, Horton JD. Molecular mediators of hepatic steatosis and liver injury. J Clin Invest 2004;114:147–152.
[25] Gavrilova O, Haluzik M, Matsusue K, Cutson JJ, Johnson L, Dietz KR, et al. Liver peroxisome proliferator-activated receptor gamma contributes to hepatic steatosis, triglyceride clearance, and regulation of body fat mass. J Biol Chem 2003;278:34268–34276.
[26] Laplante M, Sabatini DM. An emerging role of mTOR in lipid biosynthesis. Curr Biol 2009;19:R1046–R1052.
[27] Patek PQ, Collins JL, Cohn M. Transformed cell lines susceptible or resistant to in vivo surveillance against tumorigenesis. Nature 1978;276:510–511.
[28] Sakurai T, He G, Matsuzawa A, Yu G-Y, Maeda S, Hardiman G, et al. Hepatocyte necrosis induced by oxidative stress and IL-1α release mediate carcinogen-induced compensatory proliferation and liver tumorigenesis. Cancer Cell 2008;14:156–165.
[29] Ogasawara J, Watanabe-Fukunaga R, Adachi M, Matsuzawa A, Kasugai T, Kitamura Y, et al. Lethal effect of the anti-Fas antibody in mice. Nature 1993;364:806–809.
[30] Gymnopoulos M, Elsliger MA, Vogt PK. Rare cancer-specific mutations in PIK3CA show gain of function. Proc Natl Acad Sci USA 2007;104:5569–5574.
[31] Aoki M, Batista O, Bellacosa A, Tsichlis P, Vogt PK. The Akt kinase: molecular determinants of oncogenicity. Proc Natl Acad Sci USA 1998;95:14950–14955.
[32] Zender L, Xue W, Zuber J, Semighini CP, Krasnitz A, Ma B, et al. An oncogenomics-based in vivo RNAi screen identifies tumor suppressors in liver cancer. Cell 2008;135:852–864.
[33] Xue W, Krasnitz A, Lucito R, Sordella R, Vanaelst L, Cordon-Cardo C, et al. DLC1 is a chromosome 8p tumor suppressor whose loss promotes hepatocellular carcinoma. Genes Dev 2008;22:1439–1444.
[34] Zeng Q, Hong W. The emerging role of the hippo pathway in cell contact inhibition, organ size control, and cancer development in mammals. Cancer Cell 2008;13:188–192.
[35] Ishii H, Horie Y, Ohshima S, Anezaki Y, Kinoshita N, Dohmen T, et al. Eicosapentaenoic acid ameliorates steatohepatitis and hepatocellular carcinoma in hepatocyte-specific Pten-deficient mice. J Hepatol 2009;50:562–571.

[36] Suganami T, Tanimoto-Koyama K, Nishida J, Itoh M, Yuan X, Mizuarai S, et al. Role of the Toll-like receptor 4/NF-kappaB pathway in saturated fatty acid-induced inflammatory changes in the interaction between adipocytes and macrophages. Arterioscler Thromb Vasc Biol 2007;27:84–91.
[37] Vinciguerra M, Veyrat-Durebex C, Moukil MA, Rubbia-Brandt L, Rohner-Jeanrenaud F, Foti M. PTEN down-regulation by unsaturated fatty acids triggers hepatic steatosis via an NF-kappaBp65/mTOR-dependent mechanism. Gastroenterology 2008;134:268–280.
[38] Vinciguerra M, Sgroi A, Veyrat-Durebex C, Rubbia-Brandt L, Buhler LH, Foti M. Unsaturated fatty acids inhibit the expression of tumor suppressor phosphatase and tensin homolog (PTEN) via microRNA-21 up-regulation in hepatocytes. Hepatology 2009;49:1176–1184.
[39] Hatanaka H, Tsukui M, Takada S, Kurashina K, Choi YL, Soda M, et al. Identification of transforming activity of free fatty acid receptor 2 by retroviral expression screening. Cancer Sci 2010;101:54–59.
[40] Kang S, Bader AG, Vogt PK. Phosphatidylinositol 3-kinase mutations identified in human cancer are oncogenic. Proc Natl Acad Sci USA 2005; 102:802–807.
[41] Pettinelli P, Videla LA. Up-regulation of PPAR-γ mRNA expression in the liver of obese patients: an additional reinforcing lipogenic mechanism to SREBP-1c induction. J Clin Endocrinol Metab 2011;96:1424–1430.
[42] Blanco-Aparicio C, Renner O, Leal JF, Carnero A. PTEN, more than the AKT pathway. Carcinogenesis 2007;28:1379–1386.
[43] Li G, Robinson GW, Lesche R, Martinez-Diaz H, Jiang Z, Rozengurt N, et al. Conditional loss of PTEN leads to precocious development and neoplasia in the mammary gland. Development 2002;129:4159–4170.
[44] Ackler S, Ahmad S, Tobias C, Johnson MD, Glazer RI. Delayed mammary gland involution in MMTV-AKT1 transgenic mice. Oncogene 2002;21: 198–206.
[45] Hutchinson J, Jin J, Cardiff RD, Woodgett JR, Muller WJ. Activation of Akt (protein kinase B) in mammary epithelium provides a critical cell survival signal required for tumor progression. Mol Cell Biol 2001;21:2203–2212.
[46] Tamura M, Gu J, Matsumoto K, Aota S, Parsons R, Yamada KM. Inhibition of cell migration, spreading, and focal adhesions by tumor suppressor PTEN. Science 1998;280:1614–1617.
[47] Jia S, Liu Z, Zhang S, Liu P, Zhang L, Lee SH, et al. Essential roles of PI(3)K-p110beta in cell growth, metabolism and tumorigenesis. Nature 2008;454: 776–779.
[48] Day CP, James OF. Steatohepatitis: a tale of two "hits"? Gastroenterology 1998;114:842–845.
[49] Malaguarnera L, Madeddu R, Palio E, Arena N, Malaguarnera M. Heme oxygenase-1 levels and oxidative stress-related parameters in non-alcoholic fatty liver disease patients. J Hepatol 2005;42:585–591.

Journal of Gastroenterology and Hepatology

JGHF

doi:10.1111/j.1440-1746.2010.06559.x

HEPATOLOGY

Utility of contrast-enhanced ultrasonography with Sonazoid in radiofrequency ablation for hepatocellular carcinoma

Ryota Masuzaki,* Shuichiro Shiina,* Ryosuke Tateishi,* Haruhiko Yoshida,* Eriko Goto,* Yosuke Sugioka,† Yuji Kondo,* Tadashi Goto,* Hitoshi Ikeda,† Masao Omata‡ and Kazuhiko Koike*

*Graduate School of Medicine, Department of Gastroenterology, The University of Tokyo, †Department of Clinical Laboratory, The University of Tokyo Hospital, Tokyo ‡Yamanashi Prefectural Hospital Organization, Kofu, Japan

Key words
contrast-enhanced ultrasonography, hepatocellular carcinoma, radiofrequency ablation.

Accepted for publication 23 October 2010.

Correspondence
Haruhiko Yoshida, Department of Gastroenterology, University of Tokyo, 7-3-1 Hongo, Bunkyo-ku, Tokyo 113-8655, Japan.
Email: yoshida-2im@h.u-tokyo.ac.jp

The authors do not have any financial or other relationships to disclose.

Abbreviations
CEUS, contrast-enhanced ultrasonography; CT, computed tomography; HCC, hepatocellular carcinoma; RFA, radiofrequency ablation; US, ultrasonography.

Abstract

Background and Aims: Kupffer imaging in contrast-enhanced ultrasonography (CEUS) with Sonazoid, which lasts for 60 min or longer, may be useful in ultrasound-guided percutaneous tumor ablation. The utility of Sonazoid in radiofrequency ablation (RFA) of hepatocellular carcinoma (HCC) was investigated in this study.
Methods: We analyzed a total of 716 HCC nodules that were detected on dynamic computed tomography in 316 patients. Detectability of these nodules was compared between CEUS and conventional ultrasonography. The effectiveness in the treatment was assessed by comparing the mean numbers of treatment sessions of RFA in patients treated with CEUS and that in historical controls matched for tumor and background conditions.
Results: Detectability of tumor nodule was 83.5% in conventional ultrasonography and 93.2% in CEUS ($P = 0.04$). Sixty-nine nodules in 52 patients were additionally detected with CEUS. The number of additionally detected tumor nodules was positively correlated with serum albumin level ($P = 0.016$). The number of RFA sessions was 1.33 ± 0.45 with CEUS as compared to 1.49 ± 0.76 in the historical controls ($P = 0.0019$).
Conclusions: CEUS with Sonazoid is useful for HCC detection in patients with a well-conserved liver function reservoir. The decrease in RFA session numbers indicated the utility of Sonazoid in RFA treatment of HCC.

Introduction

Hepatocellular carcinoma (HCC) is the sixth most common cancer worldwide and the third most frequent cause of cancer death.[1] Because potentially curative treatments can be indicated only at less advanced stages, detection of HCC at an early stage is still a prerequisite for improved prognosis.[2] Recently, radiofrequency ablation (RFA) has been introduced and accepted as an effective nonsurgical treatment for HCC,[3–5] showing 5-year survival rates exceeding 50%.[6] RFA is potentially curative, minimally invasive, and easily repeatable in case of recurrence.

Real-time visualization of the target lesion is sine qua non for percutaneous ultrasound-guided ablation therapies, including RFA. However, visualization is sometimes difficult because of shape changes and coarse parenchymal echogenicity in cirrhotic liver.[7] Virtual sonographic images reconstructed from multidetector-row computed tomography (CT) images are useful for HCC nodules that are not depicted by conventional ultrasonography (US).[8] However, virtual sonographic images do not always precisely correspond to the real-time US images because of locational and morphological changes in the liver caused by respiration, postural movement, or bowel peristalsis. Although CT-guided RFA is thought to be useful for such nodules, real-time visualization is inferior to US guidance and accompanied by radiation exposure to operators and patients.[9] Several contrast materials have been developed to improve US resolution and have indeed been shown to be useful in differential diagnosis of hepatic tumorous lesions.[10,11] However, their role in percutaneous ablation is limited because of the short-lasting enhancement effect.

A second-generation sonographic contrast agent, Sonazoid (Daiichi-Sankyo, Tokyo, Japan), a lipid stabilized suspension of perfluorobutane gas microbubbles, has been used clinically in Japan since January 2007 in patients with liver tumors, with phase inversion harmonic gray scale sonography.[12,13] The perfluorobutane microbubbles are taken up by Kupffer cells in the liver sinusoid, allowing parenchyma-specific imaging of the liver. This imaging, called Kupffer imaging, is typically presented 10 min after injection of Sonazoid, when lesions that contain few Kupffer cells are clearly delineated as contrast defect surrounded by enhanced normal hepatic parenchyma. Kupffer imaging is particularly useful in detecting HCC nodules, which typically lack Kupffer cells. Moreover, contrast-enhanced ultrasonography

(CEUS) with Sonazoid can be expected to be useful also in ultrasound-guided percutaneous ablation, including RFA, because Kupffer imaging lasts usually for more than 60 min. However, there are few reports about the utility of Sonazoid as a contrast agent during RFA of HCC.[14,15]

The aim of the present study was to evaluate the utility of the contrast agent Sonazoid in ultrasound-guided percutaneous RFA of HCC in terms of HCC nodule detection. Overall facilitation of the ablation procedure was also evaluated by comparing the numbers of RFA sessions per treatment between RFA using CEUS with Sonazoid and matched historical controls that had used conventional US.

Methods

Patients

We analyzed a total of 716 HCC nodules in 316 consecutive patients who were admitted for RFA between July 2007 and December 2007. All patients were treated on an inpatient basis. In every case, CEUS was carried out the day before RFA. Detection of HCC nodules was compared between CEUS and conventional US, using dynamic CT as the reference standard. In 291 patients, CEUS was carried out also during RFA. We assessed whether CEUS facilitated RFA by comparing the numbers of RFA sessions per treatment in CEUS-assisted RFA and in historical controls matched for tumor and background conditions, performed with conventional US between January 2004 and July 2007. The study protocol conformed to the ethical guidelines of the Helsinki Declaration 2004 and was approved by the research ethics committee of the authors' institution.

Diagnosis of HCC

HCC was diagnosed by dynamic CT, considering hyperattenuation in the arterial phase with washout in the late phase as a definite finding.[16] Multidetector-row CT (MDCT) was performed within a month before RFA, where plain and dynamic contrast-enhanced CT images were obtained with rapid intravenous injection of a contrast material. MDCT systems used for our study were Aquillion 64 (Toshiba, Tokyo, Japan) or LightSpeed VCT (GE Healthcare, Milwaukee, WI, USA). A bolus of iodinated contrast material was injected using a mechanical power injector in 30 s, at a concentration of 300–370 mg I/mL for the amount of bodyweight (kg) × 2 mL (maximum, 100 mL). The three contrast-enhanced phases (early arterial phase, late arterial phase, and equilibrium phase) were obtained at 25, 40, and 120 s after the start of injection. Reconstruction images were obtained with a section thickness of 2.5 mm with a reconstruction interval of 1.5 mm. Most HCC nodules were also confirmed histopathologically with ultrasound-guided biopsy afterwards. The pathological grade was evaluated based on Edmondson–Steiner criteria.[17]

Ultrasound examinations

All US examinations were carried out using the SSA-770A apparatus (APLIO; Toshiba, Tokyo, Japan), on patients after at least 5 h of fasting. First, we examined the liver for HCC lesions with conventional tissue harmonic imaging. We performed both intercostal and subcostal scans of the right lobe, and both sagittal and transverse scans of the left lobe. Efforts were exerted to maximize visualization of lesions, including positional changes and breath holding. Then, CEUS was performed by the same operator with phase inversion mode imaging. A 0.5-mL dose of Sonazoid was injected into an antebrachial vein at 0.2 mL/s via a 21-gauge cannula, followed by 20-mL of normal saline. The whole liver was scanned with CEUS, using similar techniques as used in the conventional US, 10 min after Sonazoid injection. When visualization was not sufficient at that time, a CEUS scan was repeated after a 5–10-min interval. Findings in conventional US and CEUS were separately recorded by the operator. Detection ability of US and CEUS was calculated using dynamic CT as a reference standard. We analyzed the correlation between the number of additionally detected nodules by CEUS and liver function reservoir, as represented by serum albumin concentration.

RFA sessions

Inclusion criteria for percutaneous ablation were as follows: total bilirubin concentration lower than 3 mg/dL; platelet count not less than $50 \times 10^3/mm^3$; and prothrombin activity not lower than 50%. Patients with portal vein tumor thrombosis, refractory ascites, or extrahepatic metastasis were excluded. The procedure has been meticulously described elsewhere.[18] In brief, grounding was achieved by attaching two pads to the patient's thighs. A 17-gauge, cooled-tip electrode with a 2- or 3-cm exposed tip was attached to a radiofrequency generator (Covidien, Mansfield, MA, USA). After local anesthesia, the electrode was inserted under ultrasound guidance. During ablation, the temperature was measured with a thermocouple in the electrode and tissue impedance was also monitored by a circuitry incorporated into the generator. A peristaltic pump infused 0°C saline into the electrode lumen to maintain the tip temperature below 20°C. Radiofrequency energy was delivered for 6–12 min on each application. A 12-min ablation using a 3-cm electrode would produce a quasi-spherical necrotic volume 3 cm in diameter. For larger lesions, the electrode was repeatedly inserted into different sites, so that the entire lesion could be enveloped by assumed necrotic volumes.

CEUS-assisted RFA was done basically with Kupffer imaging at least 10 min after Sonazoid injection. Electrodes were inserted after perfluorobutane microbubbles disappeared from vessels so that the vessels were well visualized. Before the introduction of CEUS, when a nodule was not well visualized by conventional US, the needle was inserted by real-time ultrasound reference to the portal vein or hepatic vein near the target nodule.

The efficacy of RFA was assessed with contrast-enhanced CT performed on the next day. Complete ablation was defined as hypoattenuation of each lesion with a sufficient safety margin in the surrounding liver parenchyma. When ablation was found to be insufficient, an additional session of RFA was carried out, until complete ablation was confirmed on contrast-enhanced CT. The number of RFA sessions was defined as the total number of intervention episodes required to achieve complete ablation.

Follow up

Each patient was followed up with contrast-enhanced CT every 4 months. Tumor recurrence was diagnosed according to the

same criteria applied to initial HCC diagnosis. Intrahepatic recurrence was classified as either recurrence at a site distant from the primary site or that adjacent to the treated lesion (local tumor progression).

Historical controls

One historical control was selected for each patient who underwent CEUS-assisted RFA from patients who received RFA between January 2004 and July 2007, that is, prior to the introduction of CEUS ($n = 2261$). The maximum diameter of tumors (± 0.3 cm), the number of lesions (exact), viral markers (exact), and serum albumin concentration (± 0.3 g/dL) were used as the matching factors, with the maximum permissible differences shown in parentheses. The selection was carried out using the find-matches function of S-Plus 2000 (TIBCO Software, Palo Alto, CA, USA).

Statistical analysis

Variables were expressed as mean ± standard deviation unless otherwise specified. Continuous variables were compared using the unpaired Student's *t*-test, and categorical variables were compared using Fisher's exact probability test. The number of RFA sessions per patient was compared using the Mann–Whitney *U*-test. All tests were two-sided with a significance level of 5%. Statistical analyses were carried out with S-plus 2000.

Results

The baseline characteristics of patients who underwent CEUS are shown in Table 1. The patients consisted of 216 men and 100 women with a mean age of 70.1 ± 7.7 years. The mean maximum diameter of tumors was 1.6 ± 0.8 cm. All 316 patients underwent both conventional US and CEUS, in this order, the day before scheduled RFA. Of 716 HCC nodules diagnosed on dynamic CT, conventional US identified 598 (83.5%) nodules as definite lesions. Subsequent CEUS detected an additional 69 nodules, increasing the detectability to 93.2%, and the difference was statistically significant ($P = 0.04$). The number of additionally detected nodules per patient was one in 36 patients, two in eight, three in five, and more than three in three; thus at least one nodule was additionally detected with CEUS in a total of 52 patients (16.5%). Among these patients, artificial pleural effusion was used in 19 cases and artificial ascites was used in four patients, resulting in additional detection of 28 and four nodules, respectively. The number of additionally detected nodules by CEUS was positively correlated with serum albumin concentration ($P = 0.016$) (Fig. 1).

CEUS was also used during the RFA session in 291 patients. Artificial pleural effusion was performed in 71 (24.4%) cases and artificial ascites was used in 27 (9.1%) cases. Two demonstrative cases successfully treated with CEUS-assisted RFA are shown in Figures 2 and 3. We did not conduct randomization on the use of CEUS because its usefulness in tumor visualization was obvious at least in a proportion of the patients. Instead, we chose historical controls matched for tumor-related factors and liver function, and compared the number of RFA sessions per patient and total ablation time per session. In all patients including controls, RFA sessions were repeated until complete ablation of each nodule was confirmed on contrast-enhanced CT. The mean number of RFA sessions per patient was 1.33 ± 0.45 in patients with CEUS, as compared to 1.49 ± 0.76 in the historical controls ($P = 0.0019$ by Mann–Whitney *U*-test) (Table 2). Total ablation time per session was 17.2 ± 10.7 min with CEUS-assisted RFA and 15.7 ± 9.6 min in the historical controls ($P = 0.156$ by Mann–Whitney *U*-test). Treatment-related complications occurred in six patients (1.9%) who received CEUS-assisted RFA: peritoneal bleeding in three patients and hemothorax, bile duct bleeding, and dermal burn each in one patient. There was no treatment-related death. The incidence of complications did not differ in the historical controls (1.7%, $P = 0.867$ by Fisher's exact probability test). During the follow up, local tumor progression was detected in six patients (2.1%) who received CEUS-assisted RFA and in eight

Table 1 Baseline characteristics ($n = 316$)

Variables	
Age (years)†	70.1 ± 7.7
Male, *n* (%)	216 (68.3)
HBsAg positive, *n* (%)	45 (14.2)
HCVAb positive, *n* (%)	238 (75.3)
Diameter (cm)†	1.6 ± 0.8
Number of tumors	
1, *n* (%)	124 (39.3)
2–3, *n* (%)	143 (45.2)
≥ 4, *n* (%)	49 (15.5)
Total bilirubin (mg/dL)‡	0.9 (0.6–1.2)
Albumin (g/dL)‡	3.6 (3.2–3.9)
Platelet count (10^4/mm^3)‡	10.5 (7.3–13.8)
AFP (ng/mL)‡	16.9 (6.0–62.8)
L3 (%)‡	0.5 (0–3.1)
DCP (mAU/mL)‡	20 (13–50)

†Mean ± standard deviation.
‡Median (25th–75th percentiles).
AFP, alpha-fetoprotein; DCP, des-gamma-carboxy-prothrombin; HBsAg, hepatitis B surface antigen; HCVAb, hepatitis C virus antibody.

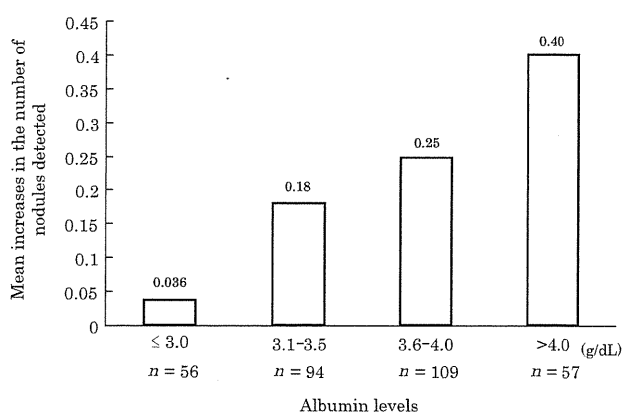

Figure 1 The mean increases in detected tumor number with contrast-enhanced ultrasonography were well correlated with serum albumin level ($P = 0.016$).

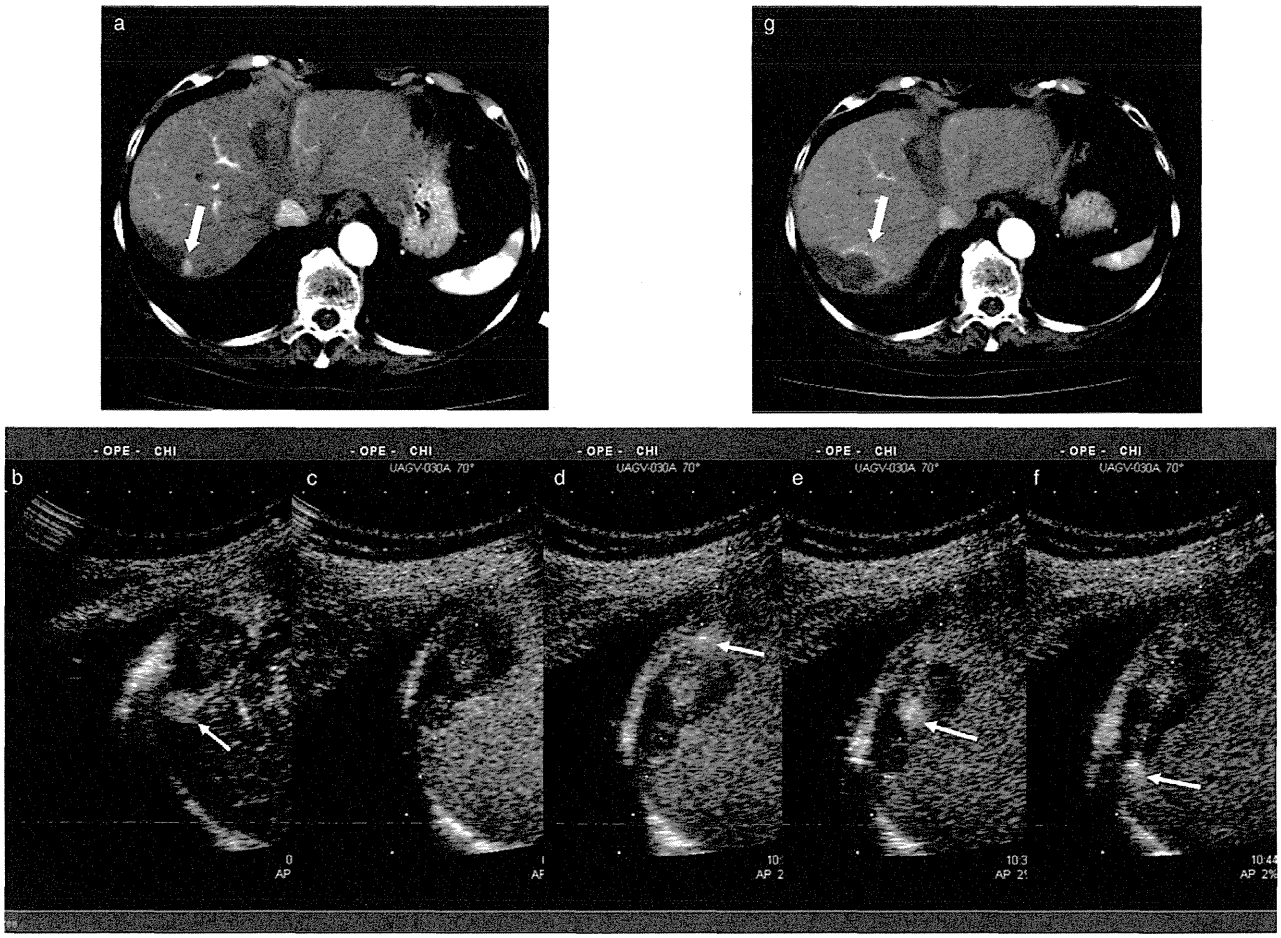

Figure 2 (a) An 80-year-old woman with hepatocellular carcinoma. Computed tomography (CT) revealed a nodule with hyperattenuation in the early arterial phase near a previously ablated lesion. (b) After injection of Sonazoid with artificial right pleural effusion, the nodule was clearly detected as a hyperechoic lesion (arrows). (c–f) Radiofrequency ablation of the nodule. (Arrows indicate the tip of radiofrequency needle). (g) Evaluation CT confirmed that the nodule was sufficiently ablated.

historical controls (2.7%, $P = 0.788$ by Fisher's exact probability test).

Discussion

In the present study, we have shown that the number of RFA sessions required per patient was significantly decreased when using the new US contrast agent, Sonazoid, as compared to historical controls. These were accomplished without increasing the incidence of local tumor progression or treatment-related complications. At the authors' institution, RFA is repeated until complete ablation of each HCC nodule is confirmed by dynamic CT. Without CEUS, when the tumor was not well delineated on conventional US, ablation used to be performed based on the information on CT and indecisive US images, which may have led to insufficient ablation revealed by evaluation CT, requiring an additional ablation session. Thus it can be assumed that the decreased number of RFA sessions with Sonazoid is mainly due to improvement in tumor detection and delineation. Unnecessary ablation of non-cancerous liver parenchyma may have deleterious effects on liver function and may reduce survival time. Thus the decrease in the number of RFA sessions is beneficial not only in cost reduction but possibly also for patients' survival.

The detectability of HCC nodules was increased from 83.5% to 93.2% with the use of CEUS, as determined with contrast CT as the reference standard. The benefit of using Sonazoid to detect "invisible" nodules by conventional US was more apparent in those with higher serum albumin concentration, suggesting that the resolution of Sonazoid CEUS may be compromised when liver function is substantially impaired. Uptake of perfluorobutane in non-cancerous liver depends on Kupffer cell function, which may be severely impaired in advanced liver diseases. A similar phenomenon was also reported in super paramagnetic iron oxide (SPIO)-enhanced magnetic resonance imaging.[19] Thus the contrast between HCC and non-cancerous parenchyma in Kupffer imaging can be diminished when liver function reservoir is poor. In the present study we obtained Kupffer imaging up to 30 min after

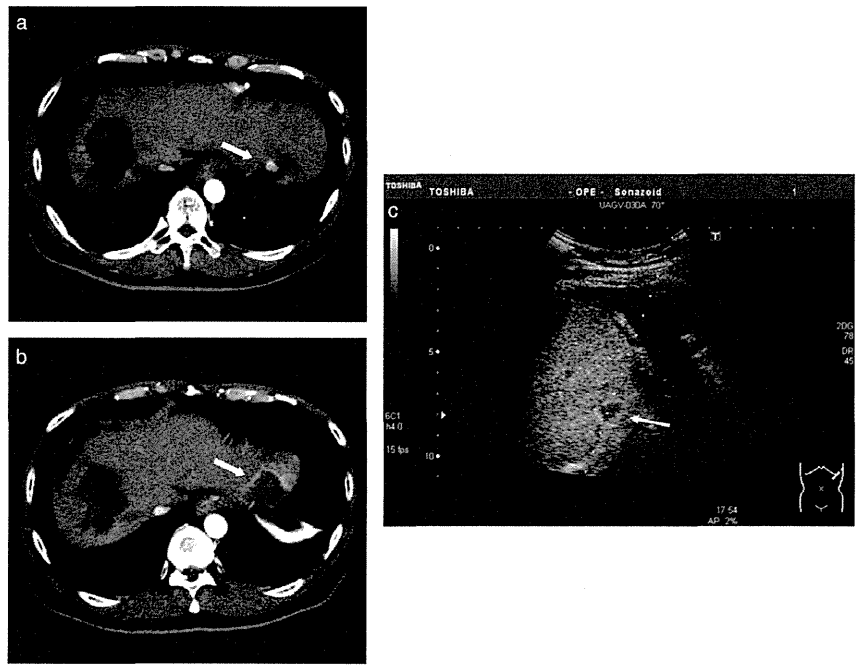

Figure 3 (a) A 52-year-old man with hepatocellular carcinoma. Computed tomography revealed a nodule at the left lateral lobe. (b) This lesion was clearly detected as an enhanced defect in the Kupffer imaging phase. Artificial left pleural effusion was used. (c) The nodule was sufficiently ablated.

Table 2 Comparison of the number of sessions

Variables	Contrast-enhanced ultrasonography group ($n = 291$)	Historical control group ($n = 291$)	*P* value
Maximum diameter (cm)†	1.9 ± 0.8	1.9 ± 0.8	0.94
Number of tumors†	2.1 ± 1.3	2.1 ± 1.3	1.00
Albumin‡	3.5 (3.2–3.9)	3.5 (3.2–3.9)	0.94
Platelet count‡	10.3 (7.8–11.5)	10.5 (7.3–11.3)	0.67
Ablation time per session (min)†	17.2 ± 10.7	15.7 ± 9.6	0.156
Mean number of sessions†	1.33 ± 0.45	1.49 ± 0.76	0.0019

†Mean ± standard deviation.
‡Median (25th–75th percentiles).

Sonazoid injection in cases of insufficient visualization of lesions. Uptake of perfluorobutane in liver parenchyma might have been increased with longer intervals. However, the appropriate interval for observing Kupffer imaging relative to the level of liver function level is not known. Thus, the possibility of detection failure with Sonazoid CEUS should be noted, especially in cases of advanced liver dysfunction.

During the present study, we noticed other limitations of CEUS with Sonazoid. As with conventional US, nodules in certain locations of the liver, such as those immediately below the diaphragm, are difficult to visualize clearly enough for safe and effective RFA even with Sonazoid. For such nodules, the artificial pleural effusion may be useful.[20] Artificial ascites may be useful for the demarcation of nodules near the gastrointestinal tract.[21] Indeed, in the present study, artificial pleural effusion was used in 24.4% of cases and artificial ascites was used in 9.1%, resulting in additional detection of 28 and four nodules, respectively. These techniques are useful in visualizing nodules at certain locations and may enhance the usability of CEUS.

The present study was not a randomized controlled trial directly comparing CEUS with Sonazoid and conventional US, but an analysis of utility of CEUS in RFA, which was analyzed by using historical matched controls. This study design was a compromise with the fact that the final diagnosis was based on dynamic CT, and it was unethical not to use CEUS in case of discrepancy between conventional US and dynamic CT. The historical controls were selected from HCC patients who were treated with RFA after 2004. Since that period, we have performed RFA with the same CT and US apparatuses. Precise comparison of the detection ability and resolution of HCC nodules between conventional US and CEUS will require studies with a design different from the present one.

In conclusion, CEUS with Sonazoid is useful in visualizing HCC nodules that are difficult to detect with conventional US. The number of RFA sessions required for complete ablation of every nodule was decreased in CEUS-assisted RFA, indicating that Sonazoid is a useful supportive agent in RFA. However, the effectiveness of Sonazoid may be compromised in case of severe liver dysfunction.

References

1 Parkin DM, Bray F, Ferlay J, Pisani P. Global cancer statistics, 2002. *CA Cancer J. Clin.* 2005; **55**: 74–108.
2 Bruix J, Sherman M. Management of hepatocellular carcinoma. *Hepatology* 2005; **42**: 1208–36.
3 Rossi S, Di Stasi M, Buscarini E *et al.* Percutaneous RF interstitial thermal ablation in the treatment of hepatic cancer. *AJR Am. J. Roentgenol.* 1996; **167**: 759–68.
4 Livraghi T, Goldberg SN, Lazzaroni S, Meloni F, Solbiati L, Gazelle GS. Small hepatocellular carcinoma: treatment with radio-frequency ablation versus ethanol injection. *Radiology* 1999; **210**: 655–61.
5 Shiina S, Teratani T, Obi S *et al.* A randomized controlled trial of radiofrequency ablation with ethanol injection for small hepatocellular carcinoma. *Gastroenterology* 2005; **129**: 122–30.
6 Ikai I, Arii S, Okazaki M *et al.* Report of the 17th nationwide follow-up survey of primary liver cancer in Japan. *Hepatol. Res.* 2007; **37**: 676–91.
7 Tanaka S, Kitamura T, Nakanishi K, Okuda S, Kojima J, Fujimoto I. Recent advances in ultrasonographic diagnosis of hepatocellular carcinoma. *Cancer* 1989; **63**: 1313–7.
8 Nakai M, Sato M, Sahara S *et al.* Radiofrequency ablation assisted by real-time virtual sonography and CT for hepatocellular carcinoma undetectable by conventional sonography. *Cardiovasc Intervent Radiol.* 2009; **32**: 62–9.
9 Sato M, Watanabe Y, Tokui K, Kawachi K, Sugata S, Ikezoe JC. T-guided treatment of ultrasonically invisible hepatocellular carcinoma. *Am. J. Gastroenterol.* 2000; **95**: 2102–6.
10 Fujimoto M, Moriyasu F, Nishikawa K, Nada T, Okuma M. Color Doppler sonography of hepatic tumors with a galactose-based contrast agent: correlation with angiographic findings. *AJR Am. J. Roentgenol.* 1994; **163**: 1099–104.
11 Kudo M, Tomita S, Tochio H *et al.* Sonography with intraarterial infusion of carbon dioxide microbubbles (sonographic angiography): value in differential diagnosis of hepatic tumors. *AJR Am. J. Roentgenol.* 1992; **158**: 65–74.
12 Kudo M. New sonographic techniques for the diagnosis and treatment of hepatocellular carcinoma. *Hepatol. Res.* 2007; **37** (Suppl. 2): S193–9.
13 Moriyasu F, Itoh K. Efficacy of perflubutane microbubble-enhanced ultrasound in the characterization and detection of focal liver lesions: phase 3 multicenter clinical trial. *AJR Am. J. Roentgenol.* 2009; **193**: 86–95.
14 Numata K, Morimoto M, Ogura T *et al.* Ablation therapy guided by contrast-enhanced sonography with Sonazoid for hepatocellular carcinoma lesions not detected by conventional sonography. *J. Ultrasound Med.* 2008; **27**: 395–406.
15 Minami Y, Kudo M, Hatanaka K *et al.* Radiofrequency ablation guided by contrast harmonic sonography using perfluorocarbon microbubbles (Sonazoid) for hepatic malignancies: an initial experience. *Liver Int.* 2010; **30**: 759–64.
16 Torzilli G, Minagawa M, Takayama T *et al.* Accurate preoperative evaluation of liver mass lesions without fine-needle biopsy. *Hepatology* 1999; **30**: 889–93.
17 Edmondson HA, Steiner PE. Primary carcinoma of the liver: a study of 100 cases among 48 900 necropsies. *Cancer* 1954; **7**: 462–503.
18 Tateishi R, Shiina S, Teratani T *et al.* Percutaneous radiofrequency ablation for hepatocellular carcinoma. An analysis of 1000 cases. *Cancer* 2005; **103**: 1201–9.
19 Tanimoto A, Yuasa Y, Shinmoto H *et al.* Superparamagnetic iron oxide-mediated hepatic signal intensity change in patients with and without cirrhosis: pulse sequence effects and Kupffer cell function. *Radiology* 2002; **222**: 661–6.
20 Kondo Y, Yoshida H, Tateishi R, Shiina S, Kawabe T, Omata M. Percutaneous radiofrequency ablation of liver cancer in the hepatic dome using the intrapleural fluid infusion technique. *Br. J. Surg.* 2008; **95**: 996–1004.
21 Kondo Y, Yoshida H, Shiina S, Tateishi R, Teratani T, Omata M. Artificial ascites technique for percutaneous radiofrequency ablation of liver cancer adjacent to the gastrointestinal tract. *Br. J. Surg.* 2006; **93**: 1277–82.

Research Article

EASL EUROPEAN ASSOCIATION FOR THE STUDY OF THE LIVER | JOURNAL OF HEPATOLOGY

Pathogenesis of lipid metabolism disorder in hepatitis C: Polyunsaturated fatty acids counteract lipid alterations induced by the core protein

Hideyuki Miyoshi[1], Kyoji Moriya[1], Takeya Tsutsumi[1], Seiko Shinzawa[1], Hajime Fujie[1], Yoshizumi Shintani[1], Hidetake Fujinaga[1], Koji Goto[1], Toru Todoroki[2], Tetsuro Suzuki[3], Tatsuo Miyamura[3], Yoshiharu Matsuura[4], Hiroshi Yotsuyanagi[1], Kazuhiko Koike[1,*]

[1]*Department of Internal Medicine, Graduate School of Medicine, University of Tokyo, Tokyo, Japan;* [2]*Department of Laboratory Medicine, Keio University School of Medicine, Tokyo, Japan;* [3]*Department of Virology II, National Institute of Infectious Diseases, Tokyo, Japan;* [4]*Department of Molecular Virology, Research Institute for Microbial Diseases, Osaka University, Osaka, Japan*

Background & Aims: Disturbance in lipid metabolism is one of the features of chronic hepatitis C, being a crucial determinant of the progression of liver fibrosis. Experimental studies have revealed that the core protein of hepatitis C virus (HCV) induces steatosis.

Methods: The activities of fatty acid metabolizing enzymes were determined by analyzing the fatty acid compositions in HepG2 cells with or without core protein expression.

Results: There was a marked accumulation of triglycerides in core-expressing HepG2 cells. While the oleic/stearic acid (18:1/18:0) and palmitoleic/palmitic acid ratio (16:1/16:0) were comparable in both the core-expressing and the control cells, there was a marked accumulation of downstream product, 5,8,11-eicosatrienoic acid (20:3(n-9)) in the core-expressing HepG2 cells. The addition of eicosatetraynoic acid, which inhibits delta-6 desaturase activity which is inherently high in HepG2 cells, led to a marked accumulation of oleic and palmitoleic acids in the core-expressing cells, showing that delta-9 desaturase was activated by the core protein. Eicosapentaenoic acid (20:5(n-3)) or arachidonic acid (20:4(n-6)) administration significantly decreased delta-9 desaturase activity, the concentration of 20:3(n-9), and triglyceride accumulation. This lipid metabolism disorder was associated with NADH accumulation due to mitochondrial dysfunction, and was reversed by the addition of pyruvate through NADH utilization.

Conclusions: The fatty acid enzyme, delta-9 desaturase, was activated by HCV core protein and polyunsaturated fatty acids counteracted this impact of the core protein on lipid metabolism. These results may open up new insights into the mechanism of lipid metabolism disorder associated with HCV infection and provide clues for the development of new therapeutic devices.

Keywords: Steatosis; Oleic acid; Core protein; Lipid metabolism; Desaturase; Hepatocellular carcinoma; NADH.

Received 31 March 2010; received in revised form 8 June 2010; accepted 5 July 2010; available online 22 September 2010

* Corresponding author. Address: Department of Gastroenterology, Graduate School of Medicine, University of Tokyo, 7-3-1 Hongo, Bunkyo-ku, Tokyo 113-8655, Japan. Tel.: +81 3 5800 8800; fax: +81 3 5800 8799.

E-mail address: kkoike-tky@umin.ac.jp (K. Koike).

Abbreviations: HCV, hepatitis C virus; HCC, hepatocellular carcinoma; PUFA, polyunsaturated fatty acids; PPAR, peroxisome proliferators-activated receptors; SREBP, sterol regulatory element binding protein; EPA, eicosapentaenoic acid; AA, arachidonic acid; ETYA, eicosatetraynoic acid; NADH, nicotinamide adenine dinucleotide; KBR, ketone body ratio.

Introduction

Persistent hepatitis C virus (HCV) infection leads to the development of chronic hepatitis, cirrhosis, and eventually, hepatocellular carcinoma (HCC), thereby being a serious problem worldwide both in medical and in socio-economical settings [1]. Histologically, several distinct features, such as bile duct damage, lymphoid follicle formation, and steatosis, (fatty change) characterize chronic hepatitis C [2–4]. Among these, steatosis is reproducible in experimental systems, both *in vitro* and *in vivo*, in which HCV proteins, particularly the core protein of HCV, are expressed. The introduced core gene induces the formation of lipid droplets in the cytoplasm of cultured cells [5,6], and in transgenic mice, it induces hepatic steatosis resembling that in chronic hepatitis C patients [7–10].

In addition, evidence has accumulated showing that steatosis is a crucial determining factor for the progression of liver fibrosis [11–13]. Steatosis and serum lipid profiles are also associated with sustained virological response to ribavirin/interferon combination therapy [14,15]. Moreover, HCV transgenic mice resemble chronic hepatitis C patients in terms of the development of HCC, implying that the HCV core protein is one of the most important viral molecules in the pathogenesis of hepatitis C [16,17]. It would thus be meaningful to explore the precise role of the core protein in modulating lipid metabolism, which may also be involved in hepatocarcinogenesis. More recently, involvement of the metabolism of lipids such as sphingolipids or cholesterol has been implicated in the replication of HCV, with a formation of lipid rafts, which are considered to be the place for HCV replication [18,19], hereby highlighting again the importance of lipid metabolism in HCV infection.

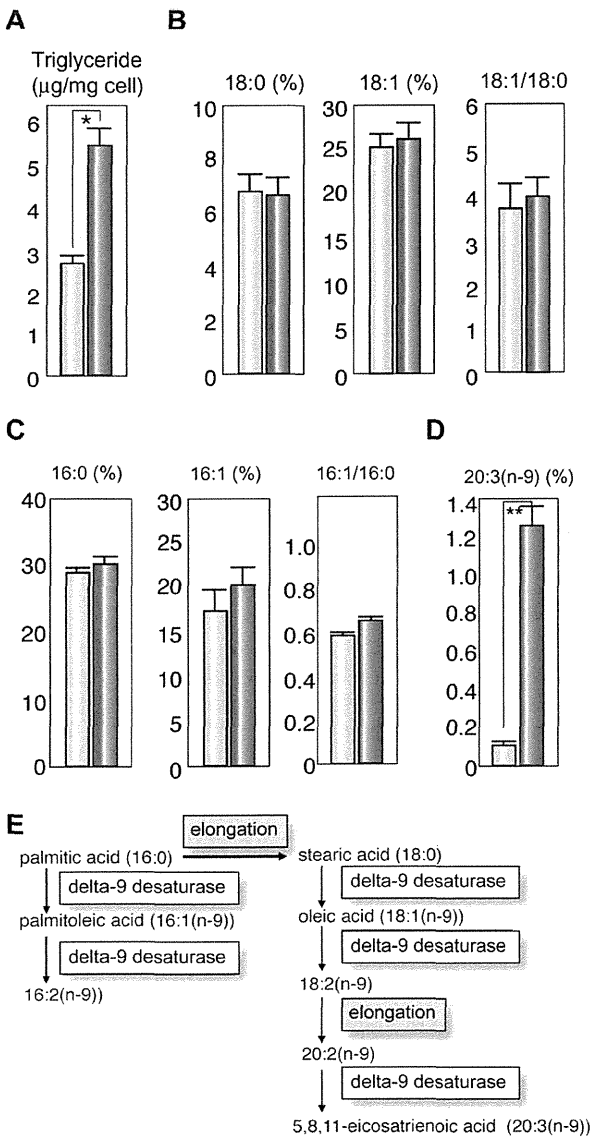

Fig. 1. Effect of the core protein on fatty acid composition in HepG2 cells. The fatty acid compositions of the total cell lipids were analyzed and the ratios of 18:1/18:0 and 16:1/16:0 in the core-expressing and control HepG2 cells were calculated. (A) Concentrations of triglycerides. (B) Percentages of stearic acid (18:0) and oleic acid (18:1(n-9)), and the 18:1/18:0 ratio. (C) Percentages of palmitic acid (16:0) and palmitoleic acid (16:1(n-9)), and the 16:1/16:0 ratio. (D) Percentage of eicosatrienoic acid (20:3(n-9). (E) Schematic display of synthetic pathway of n-9 fatty acids. Light blue bars indicate control cells and dark blue bars indicate core-expressing cells. Values represent the mean ± SE, $n = 5$ in each group. $^{*}p < 0.05$, $^{**}p < 0.01$.

Previously, we reported that the concentration of oleic acid (18:1(n-9)) was increased compared with that of stearic acid (18:0) in liver tissues of chronic hepatitis C patients as well as in those of mice transgenic for the HCV core gene [8]. Such a change may lead to increased membrane fluidity, owing to the lower melting temperature of monounsaturated fatty acids, resulting in incremental metabolism and proliferation of hepatocytes [20–22]. On the other hand, polyunsaturated fatty acids (PUFAs), such as eicosapentaenoic acid (20:5(n-3)) and arachidonic acid (20:4(n-6)), are known to activate the nuclear transcription of peroxisome proliferator-activated receptors (PPAR) and suppress the sterol regulatory element binding protein (SREBP)-1. While PPARγ induces delta-9 desaturase (stearoyl-CoA desaturase) gene expression, PUFAs suppresses delta-9 desaturase activity [23]. In the current study, we determined fatty acid desaturase activities by analyzing the fatty acid compositions in HepG2 cells expressing HCV core protein by chromatography. In addition, we determined whether exogenous PUFAs restore HCV-associated changes in fatty acid metabolism.

Materials and methods

Reagents

Eicosapentaenoic acid (EPA), arachidonic acid (AA), and eicosatetraynoic acid (ETYA) were purchased from Sigma Chemical (St. Louis, MO). Other chemicals were of analytical grade and purchased from Wako Chemicals (Tokyo, Japan).

Cell culture

This study was performed using HepG2 cell lines expressing the HCV core protein under the control of the CAG promoter (Hep39J, Hep396 and Hep397), or a control HepG2 line (Hepswx) carrying an empty vector, which were described previously [24], and control bulk HepG2 cells. They were maintained in Dulbecco's modified Eagle's medium (DMEM), supplemented with 10% fetal bovine serum (Invitrogen), 1 mg/ml G418, 100 U/ml penicillin, and 100 μg/ml streptomycin in a humidified atmosphere at 37 °C in 5% CO_2. Fatty acids were dissolved in DMEM containing defatted bovine serum albumin. The ratio of fatty acids to albumin (mole/mole) was 0.7. The cells were exposed to fatty acid–albumin complexes at various concentrations for 48 h. All the experiments were repeated at least five times.

Lipid extraction, measurement of triglyceride content, and analysis of fatty acid composition

Total cell lipids were extracted by Foch's method. The cells were washed twice with phosphate-buffered saline and collected by centrifugation. The cell pellets were homogenized with 10 vole of chloroform: methanol solution (2:1), and the mixture was shaken for 5 min. The lower phase was then washed with 4 vole of saline, dried on anhydrous sodium sulfate, and evaporated to complete dryness. For the analysis of fatty acid composition, the residue was methanolysed by the modified Morrison and Smith method with boron trifluoride as a catalyst [25]. Fatty acid methyl esters were analyzed using a Shimadzu GC-7A gas chromatograph (Shimadzu Corp., Kyoto, Japan).

Measurement of the ketone body ratio and lactate/pyruvate

The cells were cultured to confluence on 3.5 cm dishes, and the medium was replaced with 700 μl of fresh one. After 24 h of incubation, the levels of acetoacetate and β-hydroxybutyrate in the medium were measured by monitoring the production or consumption of nicotinamide adenine dinucleotide (NADH) with Ketorex kit (Sanwa Chemical, Nagoya, Japan) [26]. The ketone body ratio (KBR) was calculated as the acetoacetate/β-hydroxybutyrate ratio. The lactate and pyruvate levels in the medium were measured at random times by the lactate oxidase method and pyruvate oxidase method, respectively.

Effect of pyruvate on lipid metabolism

In some experiments, pyruvate (Wako Chemicals) was added to culture medium at a final concentration of 0, 1, 5, or 10 mM. After 48 h of incubation at 37 °C, the cells were harvested and subjected to fatty acid composition analysis or real-time PCR analysis.

Research Article

Real-time PCR

RNA was prepared from cultured cells using TRIzol LS (Invitrogen, Carlsbad, CA). The fluorescent signal was measured using ABI prism 7000 (Applied Biosystems, Tokyo, Japan). The genes encoding mouse sterol regulatory element-binding proteins (SREBP)-1a, SREBP-1c, delta-9 desaturase, and hypoxanthine phosphoribosyltransferase were amplified with the primer pairs CACAGCGGTTTTGAACGAC and CTGGCTCCTCTTTGATCCCA, ACGGAGCCATGGATTGCACATTTG and TACATCTT TAAAGCAGCGGGTGCCGATGGT, TTCCCTCCTGCAAGCTCTAC and CGCAAGAAGG TGCTAACGAAC, and CCAGCAAGCTTGCAACCTTAACCA and GTAATGATCAGTCAAC GGGGGAC, respectively.

Statistical analysis

Data are presented as the mean ± SE. The data were analyzed by Mann–Whitney *U* test. Differences were considered statistically significant when $p < 0.05$.

Results

Triglyceride content in HepG2 cells expressing HCV core protein

To validate the relationship between the lipid accumulation and the core protein, we first determined the triglyceride contents in core-protein-expressing HepG2 clones (core-expressing cells), Hep39J, Hep396, Hep397, and control HepG2 cells. Core-expressing Hep396 cells contained significantly larger amounts of triglyceride than the control cells (Fig. 1A, $p < 0.01$), which are consistent with the results of previous studies on culture cells and transgenic mice [6,7,27]. Similar results were obtained with the other core-expressing cell lines.

Fatty acid compositions of total cell lipids

Analysis on the fatty acid compositions of total lipids revealed that the concentration of oleic acid (18:1(n-9)) and the ratio of oleic acid/stearic acid (18:1/18:0) in the core-expressing cells are similar to those in the control cells (Fig. 1B). The ratio of palmitoleic acid (16:1(n-9))/palmitic acid (16:1/16:0) was higher in the core-expressing cells than that in the control cells, but the difference was not significant (Fig. 1C). This rather dissociates from the results obtained in HCV core gene transgenic mice, in which the 18:1/18:0 ratio was significantly higher than that in control mice, thereby suggesting an increased delta-9 desaturase activity as a consequence of the HCV core protein expression [8]. However, it should be noted that the concentration of 5,8,11-eicosatrienoic acid (20:3(n-9)), a downstream product of n-9 fatty acid desaturation, was approximately13 times higher in the core-expressing cells than that in the control cells (Fig. 1D and E, $p < 0.01$). This is due to the fact that the activity of the delta-6 desaturase, an enzyme downstream of delta-9 desaturase, is also high in HepG2 cells, resulting in the relatively lower concentration of 18:1 in the core-expressing cells despite the high delta-9 desaturase activity. Actually, the delta-6 desaturase activity has been shown to be inherently high in HepG2 cells [28,29].

To verify this possibility, we administered ETYA, which inhibits delta-6 desaturase activity, to the cell cultures. Because similar results were obtained with the other core-expressing HepG2 cell lines, subsequent experiments were carried out using the Hep396 cell line. The addition caused significant increases in both 18:1/18:0 and 16:1/16:0 ratios in the core-expressing cells but not in the control cells (Fig. 2A 0 vs. 10 μg/ml and 0 vs. 50 μg/ml; $p < 0.05$, respectively). When compared between the

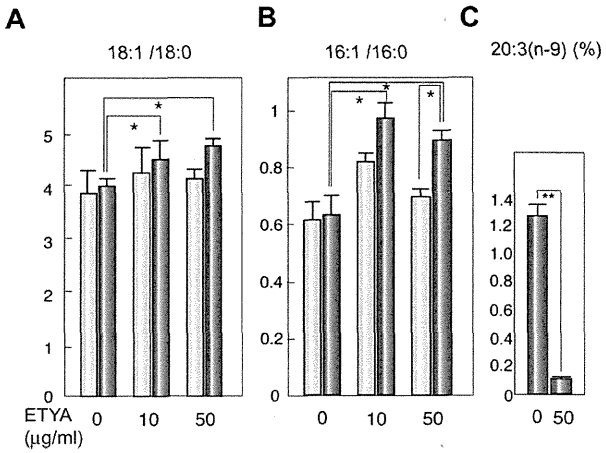

Fig. 2. Effect of ETYA on delta-9 desaturase index. HepG2 cells with or without the core protein were incubated with ETYA for 48 h. The fatty acid compositions of the total cell lipids were analyzed, and the ratios of 18:1/18:0 (A) and 16:1/16:0 (B), and the percentage of eicosatrienoic acid (20:3(n-9) (C) were computed. Light blue bars indicate control cells and dark blue bars indicate core-expressing cells. $N = 5$ in each group. *$p < 0.05$. ETYA, eicosatetraynoic acid.

core-expressing cells and control cells after the treatment with 50 μg/ml ETYA, the 18:1/18:0 ratio was higher and the 16:1/16:0 ratio was significantly higher (Fig. 2B, $p < 0.05$) in the core-expressing cells. ETYA (50 μg/ml) significantly decreased the concentration of 20:3(n-9) in the core-expressing cells (Fig. 2C, $p < 0.01$). These results suggest that the HCV core protein enhances the activities of delta-9, and possibly, delta-5 desaturases, modulating fatty acid metabolism in HepG2 cells, in which the delta-6 desaturase activity is intrinsically high (Fig. 1E) [28,29].

PUFAs modify fatty acid compositions and decrease triglyceride contents in HepG2 Cells

PUFAs are known to suppress the activities of both delta-9 and delta-6 desaturases. We, therefore, added PUFA, EPA, or AA, to the culture cell medium to examine the effect of PUFAs on the fatty acid compositions in HepG2 cells expressing the core protein. EPA and AA individually decreased the 18:1/18:0 and 16:1/16:0 ratios in a similar extent in both the core-expressing cells and the control cells (Fig. 3, $p < 0.05$). EPA and AA also significantly decreased the concentration of 20:3(n-9) in the core-expressing cells in a dose-dependent manner (Fig. 4, $p < 0.05$). In addition, EPA and AA individually decreased the triglyceride concentration in cells, in particular, in the core-expressing cells (Fig. 5, in core-expressing cells, $p < 0.01$; in control cells, $p < 0.05$, respectively).

Ketone body ratio and lactate/pyruvate ratio

Although the mechanism by which the HCV core protein enhances fatty acid desaturation is yet unclear, one possibility is the creation of an overreduced state in the core-expressing cells. The overreduced state or the accumulation of NADH in cells is known to accelerate the activities of fatty acid desaturases [30,31]. Such a condition may originate from the dysfunction of the mitochondrial electron transfer system (ETS), which has been

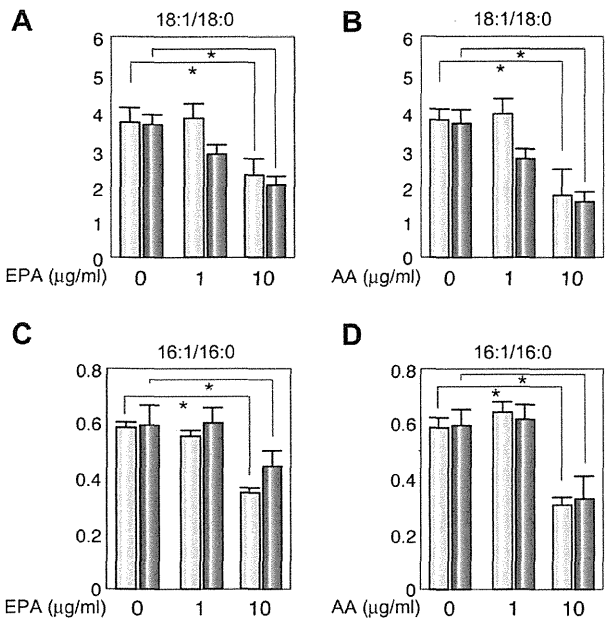

Fig. 3. Effect of EPA and AA on delta-9 desaturase index. HepG2 cells with or without the core protein were incubated with EPA (A and C) or AA (B and D) for 48 h. The fatty acid compositions of the total cell lipids were analyzed and the ratios of 18:1/18:0 (A and B) and 16:1/16:0 (C and D) were computed. Light blue bars indicate control cells and dark blue bars indicate core-expressing cells. $N = 5$ in each group. *p <0.05. EPA, eicosapentaenoic acid; AA, arachidonic acid.

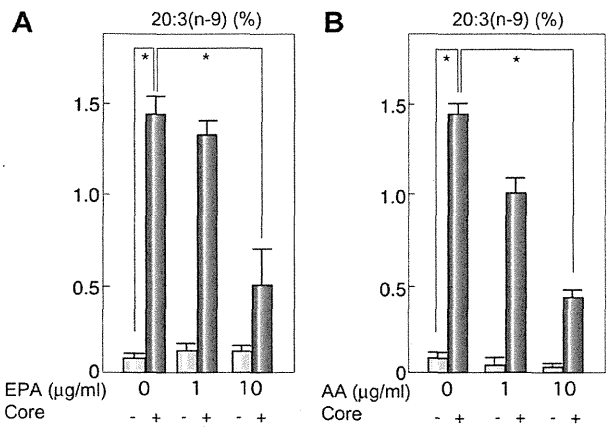

Fig. 4. Effect of EPA and AA on the concentration of 20:3(n-9). HepG2 cells with or without the core protein were incubated with EPA (A) or AA (B) for 48 h. The fatty acid compositions of the total cell lipids were analyzed and the percentages of the C20:3(n-9) fraction were measured. Light blue bars indicate control cells and dark blue bars indicate core-expressing cells. $N = 5$ in each group. *p <0.05.

suggested to be associated with HCV infection by the action of the HCV core protein [32–35]. Then, we explored the possibility that an increase in the NADH level, which is caused by the mitochondrial ETS dysfunction, induces the activation of fatty acid desaturases. Because fatty acid synthesis or fatty acid desaturation is accompanied by the oxidation of NAD(P)H, we measured the ketone body ratio (KBR) in the culture medium to estimate the redox state in the HepG2 cells expressing the core protein.

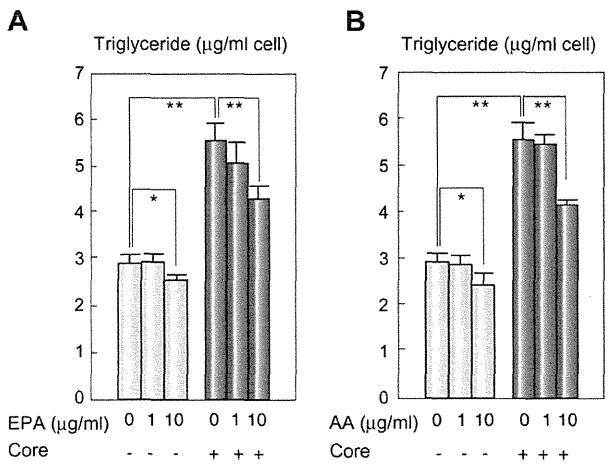

Fig. 5. Effect of EPA and AA on triglyceride content. HepG2 cells with or without the core protein were incubated with EPA (A) or AA (B) for 48 h. The triglyceride volume of the total cell lipids was measured and the triglyceride contents in the cells were calculated. Light blue bars indicate control cells and dark blue bars indicate core-expressing cells. $N = 5$ in each group. *p <0.05, **p <0.01.

The KBR, which is in equilibrium with the intramitochondrial NAD^+/NADH [26,36], in the culture medium of the core-expressing cells, was significantly lower than that of control cells (Fig. 6A, p <0.01). The ratio of lactate to pyruvate (lactate/pyruvate), which is proportional to the cytosolic NADH/NAD^+ [26], in the culture medium of the core-expressing cells was significantly higher than that of control cells (Fig. 6B, p <0.05). These results, the higher NADH/NAD^+ ratio in both determinations, indicate that NADH accumulates in the core-expressing HepG2 cells, resulting in the overreduced state, as a consequence of the core protein expression. The amounts of total ketone bodies were significantly higher in the core-expressing cells than that in the control cells (Fig. 6C).

Effects of pyruvate on lipid metabolism in core-expressing cells

The addition of pyruvate into this constitutive core protein expression system, in which the pyruvate metabolism is in equilibrium, is expected to cause a reduction in the NADH level along with increases in the levels of lactate and NAD^+, because pyruvate tends to be converted to lactate by the action of lactate dehydrogenase (LDH) under the condition of high NADH/NAD^+ ratio [26,36]. Actually, the addition of pyruvate into the culture medium at various concentrations increased the KBR and reduced the amount of 5,8,11-eicosatrienoic acid (20:3 (n-9)) (Fig. 6D, p <0.05 at 10 mM pyruvate), while it had no effect on the control cells. It also caused a reduction in the amount of triglyceride in the core-expressing cells but not in the control cells (Fig. 6E). This finding strongly supports the notion that NADH accumulation is, at least, one of the causes of the activation of fatty acid desaturases in this HCV model. The mRNA levels of anti-oxidant genes significantly decreased after the incubation with pyruvate at 10 mM (catalase, 1.27 ± 0.06 vs. 0.91 ± 0.05; glutathione synthetase 1.39 ± 0.04 vs. 1.01 ± 0.06; glutathione peroxidase 1.48 ± 0.03 vs. 1.23 ± 0.07, pyruvate (−) vs. pyruvate (+), p <0.05, respectively), suggesting that pyruvate reduced the levels of oxidative stress in the core-expressing HepG2 cells.

Research Article

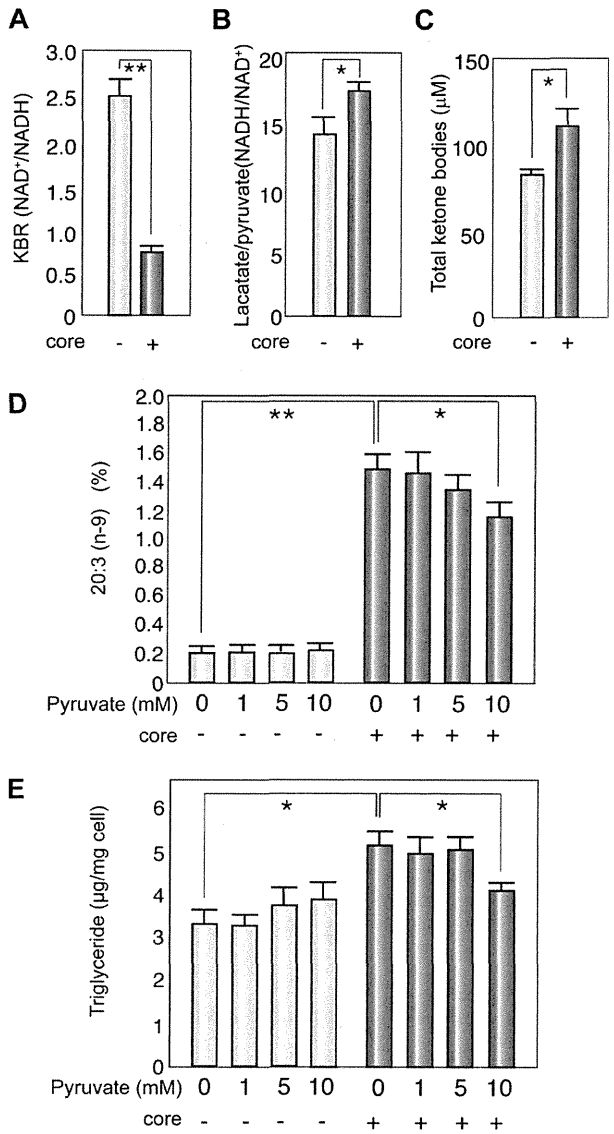

Fig. 6. NADH accumulation and effect of pyruvate in core-expressing cells. HepG2 cells with or without the core protein were subjected to the determination of ketone body ratio (A) and lactate/pyruvate ratio (B) for the precise estimation of NAD^+/NADH and NADH/NAD^+. (C) Total ketone bodies. (D) The percentages of the C20:3(n-9) fraction were measured after incubation with pyruvate at various concentrations. (E) The total amount of triglyceride was measured after incubation with pyruvate at various concentrations. Light blue bars indicate control cells and dark blue bars indicate core-expressing cells. $N = 5$ in each group. $^*p < 0.05$, $^{**}p < 0.01$.

Expression of SREBP-1 and desaturase genes in core-expressing cells

We previously showed that the core protein activates the expression of the SREBP-1c gene, which regulates the production of triglyceride [37] in the liver. We, therefore, examined the mRNA levels of genes associated with lipid metabolism in the current system. As shown in Fig. 7, the mRNA levels of SREBP-1c and delta-9 (stearoyl CoA) desaturase genes, but not that of the SREBP-1a gene, were significantly higher in the core-expressing cells than that in the control cells. Of note, the mRNA levels of the former two genes significantly decreased after the incubation with AA. The treatment with pyruvate also reduced the mRNA levels of the two genes, but the difference was not statistically significant compared with the control.

Discussion

The core protein of HCV modulated the activities of delta desaturases and changed the saturation states of fatty acids. The observed change in the HepG2 cells, namely, an increase in the amounts of unsaturated fatty acids, may support cell proliferation, by increasing the fluidity of the cell membrane as reported previously [20]. In the HepG2 cells expressing the core protein, the delta-6 desaturase activity was as high as that of the delta-9 desaturase, leading to the accumulation of a downstream product, 20:3(n-9) fatty acid. This was, unexpectedly, in contrast to our previous result on the liver tissues of HCV core gene transgenic mice, in which the 18:1/18:0 and 16:1/16:0 ratios were significantly higher than that in the liver tissues of normal littermate mice, indicating the activation of delta-9 desaturase [8]. The 16:1/16:0 and 18:1/18:0 ratios observed in the control HepG2 cells were consistent with the results of a previous study: the delta-6 desaturase activity is inherently higher in HepG2 cells than in normal mouse hepatocytes [28,29]. This may explain the difference in the effect of the core protein on lipid metabolism in these two systems, namely, HepG2 cells and mouse liver tissues. The significant increase in the delta-9 desaturase index and high concentration of 20:3(n-9) by the administration of ETYA, a delta-6 desaturase inhibitor, indicate the activation of delta-9 desaturase in the core-expressing cells. The results of real-time PCR analysis for determining the mRNA levels of these enzymes corroborated the current estimation of desaturase activities as determined by fatty acid analysis.

The mechanism underlying the activation of fatty acid desaturation by the HCV core protein is still unclear, but one possibility is the presence of an overreduced state in the core-expressing cells. The HCV core protein is closely associated with mitochondrial dysfunction, in particular, that of the respiratory chain complexes, resulting in an impairment of NADH oxidation [32–35]. NADH accumulation leads to an increase in desaturase activities through the augmentation of microsomal electron transfer [38]. In fact, the KBR in the core-expressing cells was significantly lower than that in the control cells, indicating the accumulation of NADH within the cells. The addition of pyruvate resulted in an increase in the KBR and a reduction in the amounts of triglyceride and 5,8,11-eicosatrienoic acid (20:3 (n-9)) while it had no effect on the control cells, strongly supporting the notion that NADH accumulation induced by the core protein is, at least, one of the causes of the activation of fatty acid desaturases in this HCV model.

Another possible mechanism underlying the accelerated desaturation is the activation of SREBP-1c, which controls the expression of delta-9 desaturase. In fact, the level of SREBP-1c mRNA was higher in the core-expressing cells than that in the control cells as reported previously [37]. The relief of NADH accumulation by pyruvate administration resulted in the reduced accumulation of triglyceride and unsaturated fatty acids, which was accompanied by the reduction in SREBP-1c and delta-9 desaturase gene expression levels. The intracellular accumulation of NADH might be involved in the activation of the SREBP-1c gene expression by the core protein. Thus, NADH accumulation, which

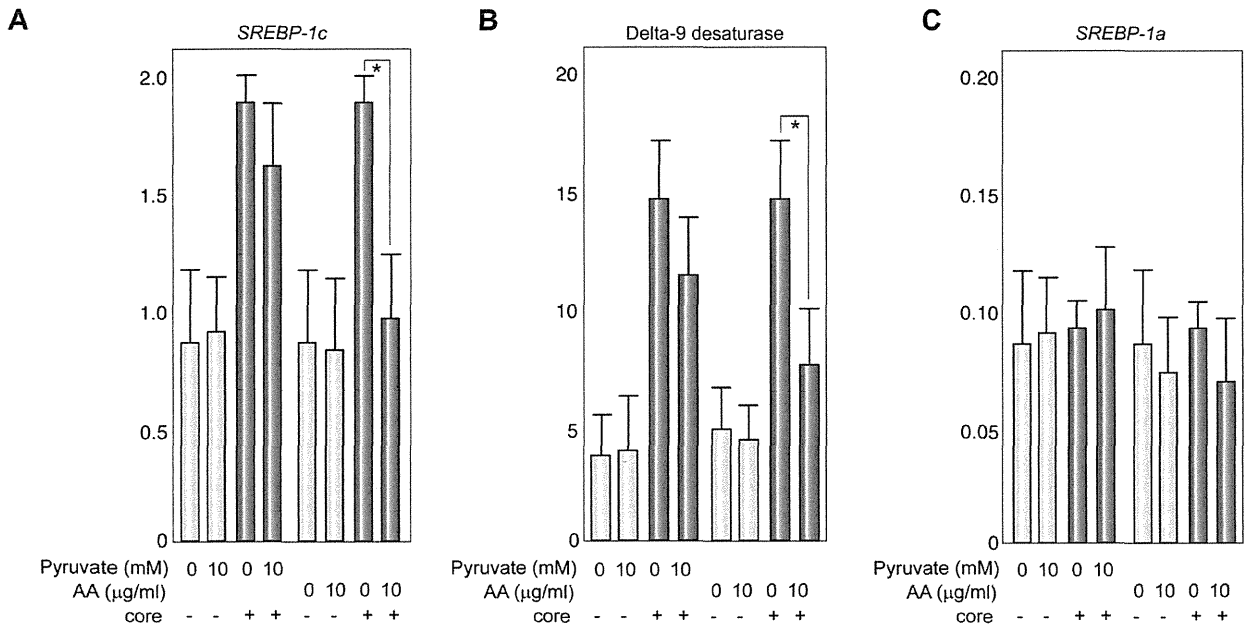

Fig. 7. Effect of pyruvate and AA on mRNA levels of lipid-associated genes. The mRNA levels of *SREBP-1c* (A), delta-9 desaturase (B) and *SREBP-1a* (C) genes were determined by real-time PCR analysis. The transcription of the genes was normalized with that of hypoxanthine phosphoribosyltransferase, and the values are expressed as relative activities. Light blue bars indicate control cells and dark blue bars indicate core-expressing cells. $N = 5$ in each group. *$p < 0.05$. SREBP, sterol regulatory element binding protein.

is induced by the core protein through the impairment of the mitochondrial complex function [35], may be a key event that leads to the SREBP-1c activation, the desaturase activation, and the development of steatosis associated with HCV infection.

EPA and AA (PUFAs), which are known to suppress desaturase activities, lowered the 18:1/18:0 and 16:1/16:0 ratios and decreased the concentration of 20:3(n-9) concomitantly with that of triglyceride, regardless of the presence of the core protein, probably through SREBP-1c suppression (Fig. 7) [39]. On the other hand, the administration of EPA or AA did not affect the KBR in the core-expressing or control cells (data not shown), limiting the PUFAs ability to counteract the effect of the core protein. This is in contrast to the fact that the addition of pyruvate caused an increase in the KBR and a reduction in the amounts of triglyceride and 5,8,11-eicosatrienoic acid (20:3 (n-9)), while it had no effect on the control cells.

Fatty acid desaturation is closely associated with increased membrane fluidity [20], leading to augmented cell metabolism and higher cell division rates [21,22]. Although the relationship between carcinogenesis and lipid metabolism altered by the HCV core protein remains to be further clarified, alterations in lipid metabolism, in particular, in the desaturation of fatty acids, are closely associated with HCV infection, and PUFAs could prevent the pathogenesis of HCV-associated disorders involving lipid metabolism.

Conflict of interest

The authors who have taken part in this study declared that they do not have anything to disclose regarding funding or conflict of interest with respect to this manuscript.

Acknowledgments

This work was supported in part by Grant-in-Aid for Scientific Research on Priority Area from the Ministry of Education, Science, Sports, and Culture of Japan; Health Sciences Research Grants of The Ministry of Health, Labour, and Welfare (Research on Hepatitis); and a grant from The Sankyo Foundation of Life Science.

References

[1] Saito I, Miyamura T, Ohbayashi A, Harada H, Katayama T, Kikuchi S, et al. Hepatitis C virus infection is associated with the development of hepatocellular carcinoma. Proc Natl Acad Sci USA 1990;87:6547–6549.
[2] Schemer PJ, Ashrafzadeh P, Sherlock S, Brown D, Dusheiko GM. The pathology of chronic hepatitis C. Hepatology 1992;15:567–571.
[3] Bach N, Thung SN, Schaffner F. The histological features of chronic hepatitis C and autoimmune chronic hepatitis: a comparative analysis. Hepatology 1992;15:572–577.
[4] Fujie H, Yotsuyanagi H, Moriya K, Shintani Y, Tsutsumi T, Takayama T, et al. Steatosis and intrahepatic hepatitis C virus in chronic hepatitis. J Med Virol 1999;59:141–145.
[5] Moradpour D, Englert C, Wakita T, Wands JR. Characterization of cell lines allowing tightly regulated expression of hepatitis C virus core protein. Virology 1996;222:51–63.
[6] Barba G, Harper F, Harada T, Kohara M, Goulinet S, Matsuura Y, et al. Hepatitis C virus core protein shows a cytoplasmic localization and associates to cellular lipid storage droplets. Proc Natl Acad Sci USA 1997;94:1200–1205.
[7] Moriya K, Yotsuyanagi H, Shintani Y, Fujie H, Ishibashi K, Matsuura Y, et al. *Hepatitis C virus core protein induces hepatic steatosis in transgenic mice.* J Gen Virol 1997;78:1527–1531.
[8] Moriya K, Todoroki T, Tsutsumi T, Fujie H, Shintani Y, Miyoshi H, et al. Increase in the concentration of carbon 18 monosaturated fatty acids in the liver with hepatitis C: analysis in transgenic mice and humans. Biophys Biochem Res Commun 2001;281:1207–1212.
[9] Lerat H, Honda M, Beard MR, Loesch K, Sun J, Yang Y, et al. Steatosis and liver cancer in transgenic mice expressing the structural and nonstructural proteins of hepatitis C virus. Gastroenterology 2002;122:352–365.

Research Article

[10] Naas T, Ghorbani M, Alvarez-Maya I, Lapner M, Kothary R, De Repentigny Y, et al. Characterization of liver histopathology in a transgenic mouse model expressing genotype 1a hepatitis C virus core and envelope proteins 1 and 2. J Gen Virol 2005;86:2185–2196.

[11] Adinolfi LE, Gambardella M, Andreana A, Tripodi MF, Utili R, Ruggiero G. Steatosis accelerates the progression of liver damage of chronic hepatitis C patients and correlates with specific HCV genotype and visceral obesity. Hepatology 2001;33:1358–1364.

[12] Massard J, Ratziu V, Thabut D, Moussalli J, Lebray P, Benhamou Y, et al. Natural history and predictors of disease severity in chronic hepatitis C. J Hepatol 2006;44:S19–S24.

[13] Leandro G, Mangia A, Hui J, Fabris P, Rubbia-Brandt L, Colloredo G, et al. HCV meta-analysis (on) individual patients' data study group. Relationship between steatosis, inflammation, and fibrosis in chronic hepatitis C: a meta-analysis of individual patient data. Gastroenterology 2006;130:1636–1642.

[14] Patton HM, Patel K, Behling C, Bylund D, Blatt LM, Vallee M, et al. The impact of steatosis on disease progression and early and sustained treatment response in chronic hepatitis C patients. J Hepatol 2004;40: 484–490.

[15] Harrison SA, Brunt EM, Qazi RA, Oliver DA, Neuschwander-Tetri BA, Di Bisceglie AM, et al. Effect of significant histologic steatosis or steatohepatitis on response to antiviral therapy in patients with chronic hepatitis C. Clin Gastroenterol Hepatol 2005;3:604–609.

[16] Moriya K, Fujie H, Shintani Y, Yotsuyanagi H, Tsutsumi T, Ishibashi K, et al. The core protein of hepatitis C virus induces hepatocellular carcinoma in transgenic mice. Nat Med 1998;4:1065–1067.

[17] Koike K. Molecular basis of hepatitis C virus-associated hepatocarcinogenesis: lessons from animal model studies. Clin Gastroenterol Hepatol 2005;3:S132–S135.

[18] Shi ST, Lee KJ, Aizaki H, Hwang SB, Lai MM. Hepatitis C virus RNA replication occurs on a detergent-resistant membrane that cofractionates with caveolin-2. J Virol 2003;77:4160–4168.

[19] Miyanari Y, Atsuzawa K, Usuda N, Watashi K, Hishiki T, Zayas M, et al. The lipid droplet is an important organelle for hepatitis C virus production. Nat Cell Biol 2007;9:1089–1097.

[20] Stubbs CD, Smith AD. The modification of mammalian membrane polyunsaturated fatty acid composition in relation to membrane fluidity and function. Biochim Biophys Acta 1984;779:89–137.

[21] Li J, Ding SF, Habib NA, Fermor BF, Wood CB, Gilmour RS. Partial characterization of a cDNA for human stearoyl-CoA desaturase and changes in its mRNA expression in some normal and malignant tissues. Int J Cancer 1994;57:348–352.

[22] Vinciguerra M, Carrozzino F, Peyrou M, Carlone S, Montesano R, Benelli R, et al. Unsaturated fatty acids promote hepatoma proliferation and progression through downregulation of the tumor suppressor PTEN. J Hepatol 2009;50:1132–1141.

[23] Ntambi JM. Regulation of stearoyl-CoA desaturase by polyunsaturated fatty acids and cholesterol. J Lipid Res 1999;40:1549–1558.

[24] Ruggieri A, Murdolo M, Harada T, Miyamura T, Rapicetta M. Cell cycle perturbation in a human hepatoblastoma cell line constitutively expressing hepatitis C virus core protein. Arch Virol 2004;149:61–74.

[25] Morrison WR, Smith LM. Preparation of fatty acid methyl esters and dimethylacetals from lipids with boron fluoride–methanol. J Lipid Res 1964;5:600–608.

[26] Williamson DH, Mellanby J, Krebs HA. Enzymic determination of D(-)-beta-hydroxybutyric acid and acetoacetic acid in blood. Biochem J 1962;82:90–96.

[27] Abid K, Pazienza V, Gottardi A, Rubbia-Brandt L, Conne B, Pugnale P, et al. An in vitro model of hepatitis C virus genotype 3a-associated triglycerides accumulation. J Hepatol 2005;42:744–751.

[28] Portolesi R, Powell BC, Gibson RA. Delta6 desaturase mRNA abundance in HepG2 cells is suppressed by unsaturated fatty acids. Lipids 2008;43:91–95.

[29] Choi Y, Park Y, Pariza MW, Ntambi JM. Regulation of stearoyl-CoA desaturase activity by the trans-10, cis-12 isomer of conjugated linoleic acid in HepG2 cells. Biochem Biophys Res Commun 2001;284:689–693.

[30] Strittmatter P, Spatz L, Corcoran D, Rogers MJ, Setlow B, Redline R. Purification and properties of rat liver microsomal stearyl coenzyme a desaturase. Proc Natl Acad Sci USA 1974;71:4565–4569.

[31] Joshi VC, Wilson AC, Wakil SJ. Assay for the terminal enzyme of the stearoyl coenzyme A desaturase system using chick embryo liver microsomes. J Lipid Res 1977;18:32–36.

[32] Korenaga M, Wang T, Li Y, Showalter LA, Chan T, Sun J, et al. Hepatitis C virus core protein inhibits mitochondrial electron transport and increases reactive oxygen species (ROS) production. J Biol Chem 2005;280: 37481–37488.

[33] Piccoli C, Scrima R, Quarato G, D'Aprile A, Ripoli M, Lecce L, et al. Hepatitis C virus protein expression causes calcium-mediated mitochondrial bioenergetic dysfunction and nitro-oxidative stress. Hepatology 2007;46:58–65.

[34] Tsutsumi T, Matsuda M, Aizaki H, Moriya K, Miyoshi H, Fujie H, et al. Proteomics analysis of mitochondrial proteins reveals overexpression of a mitochondrial protein chaperone, prohibitin, in cells expressing hepatitis C virus core protein. Hepatology 2009;50:378–386.

[35] Moriya K, Miyoshi H, Tsutsumi T, Shinzawa S, Fujie H, Shintani Y, et al. Tacrolimus ameliorates metabolic disturbance and oxidative stress caused by hepatitis C virus core protein: Analysis using mouse model and cultured cells. Am J Pathol 2009;175:1515–1524.

[36] Williamson DH, Lund P, Krebs HA. The redox state of free nicotinamide-adenine dinucleotide in the cytoplasm and mitochondria of rat liver. Biochem J 1967;103:514–527.

[37] Moriishi K, Mochizuki R, Moriya K, Miyamoto H, Mori Y, Abe T, et al. Critical role of PA28gamma in hepatitis C virus-associated steatogenesis and hepatocarcinogenesis. Proc Natl Acad Sci USA 2007;104:1661–1666.

[38] Jansson I, Schenkman JB. Studies on three microsomal electron transfer enzyme systems. Specificity of electron flow pathways. Arch Biochem Biophys 1977;178:89–107.

[39] Sekiya M, Yahagi N, Matsuzaka T, Najima Y, Nakakuki M, Nagai R, et al. Polyunsaturated fatty acids ameliorate hepatic steatosis in obese mice by SREBP-1 suppression. Hepatology 2003;38:1529–1539.

Living Donor Liver Transplantations in HIV- and Hepatitis C Virus-Coinfected Hemophiliacs: Experience in a Single Center

Kunihisa Tsukada,[1,2] Yasuhiko Sugawara,[3,10] Junichi Kaneko,[3] Sumihito Tamura,[3] Natsuo Tachikawa,[2,4] Yuji Morisawa,[1,5] Shu Okugawa,[1] Yoshimi Kikuchi,[2] Shinichi Oka,[2] Satoshi Kimura,[1,2,6] Yutaka Yatomi,[7] Masatoshi Makuuchi,[8] Norihiro Kokudo,[3] and Kazuhiko Koike[1,9]

Background. Although almost all human immunodeficiency virus (HIV)-infected Japanese hemophiliacs are coinfected with hepatitis C virus (HCV), the outcome of living donor liver transplantation (LDLT) in such patients in terms of survival rate, perioperative complications, and recovery of coagulation activity is poorly understood.
Patients and Methods. Six HIV-positive hemophiliacs underwent LDLT for HCV-associated advanced cirrhosis. The mean CD4 T-cell count at transplantation was 376±227/μL.
Results. The 1-, 3-, and 5-year survival rates were 66%, 66%, and 50%, respectively. Fatal perioperative bleeding related to hemophilia was not observed. Two patients died within 6 months after transplantation due to graft failure. HIV infection was well controlled in all patients who survived longer than 6 months. Two patients (genotype 2a and 2+3a) achieved a sustained viral response and both of them were alive at the end of follow-up period, whereas one patient (genotype 1a+1b) died of decompensated cirrhosis 4 years after transplantation due to recurrent HCV infection.
Conclusions. HIV/HCV-coinfected hemophiliacs can safely undergo LDLT. Hemophilia was clinically cured after successful transplantation. A good outcome can be expected as long as postoperative hepatitis C is controlled with interferon/ribavirin combination therapy.

Keywords: Hepatitis C virus, Living donor liver transplantation, HIV, HAART.

(*Transplantation* 2011;91: 1261–1264)

Because of the availability of highly active antiretroviral therapy (HAART), the life expectancy of patients infected with human immunodeficiency virus (HIV) has dramatically improved (*1*). Death from opportunistic infections has decreased and, as the result, non-acquired immune deficiency syndrome (AIDS)-defining complications such as hepatic diseases, cardiovascular diseases, or non-AIDS malignancies have emerged as the most important problems (*2*, *3*).

Hepatitis C virus (HCV) and HIV often coinfect due to their shared route of transmission. A recent report indicated that approximately 20% of HIV-infected people in Japan are coinfected with HCV (*4*), a large proportion of whom are hemophiliacs. Approximately 1500 hemophiliacs were infected with HIV through non heat-treated concentrated coagulation factor administration between 1981 and 1985, and 98% of them were also infected with HCV. The coexistence of HIV infection with HCV accelerates the progression of liver fibrosis (*5*) and attenuates the efficacy of interferon (IFN) treatment for HCV (*6*, *7*). A considerable number of such coinfected patients suffer from decompensated cirrhosis or hepatocellular carcinoma (HCC) (*8*). In the HAART era, AIDS-related death is gradually decreasing (*9*) and HCV-

This work was supported by a Grant-in-aid for Scientific Research from the Ministry of Education, Culture, Sports, Science and Technology of Japan and from the Ministry of Health, Labor and Welfare of Japan (AIDS Research).
[1] Department of Infectious Diseases, Graduate School of Medicine, the University of Tokyo, Bunkyo-Ku, Tokyo.
[2] AIDS Clinical Center, National Center for Global Health and Medicine, Shinjuku-ku, Tokyo, Japan.
[3] Division of Artificial Organ and Transplantation, Department of Surgery, the University of Tokyo, Bunkyo-Ku, Tokyo.
[4] Yokohama Municipal Citizens Hospital, Yokohama, Japan.
[5] Department of Infection Control, Jichi Medical School, Tochigi-ken, Japan.
[6] Tokyo Teishin Hopital, Chiyoda-ku, Tokyo, Japan.
[7] Department of Clinical Laboratory Medicine, the University of Tokyo, Bunkyo-Ku, Tokyo.
[8] Japanese Red Cross Hospital, Shibuya-Ku, Tokyo, Japan.
[9] Department of Gastroenterology, Graduate School of Medicine, the University of Tokyo, Bunkyo-Ku, Tokyo.
[10] Address correspondence to: Yasuhiko Sugawara, M.D., Division of Artificial Organ and Transplantation, Department ofSurgery, University of Tokyo, 7-3-1 Hongo, Bunkyo-Ku, Tokyo.
E-mail: yasusugatky@yahoo.co.jp
K.T., Y.S., J.K., S.T., Y.Y., M.M., N.K., and K.K. participated in research design; K.T. and Y.S. participated in the writing of the manuscript; and N.T., Y.M., S.O., Y.K., S.O., and S.K. participated in the performance of the research.
Received 2 December 2010. Revision requested 3 January 2011.
Accepted 7 March 2011.

ISSN 0041-1337/11/9111-1261
DOI: 10.1097/TP.0b013e3182193cf3